Development and Comparison of Empirical Models for All-sky Downward Longwave Radiation Estimation at the Ocean Surface Using Long-term Observations

Jianghai Peng[1,2,3,4], Bo Jiang[1,2]*, Hui Liang[1,2], Shaopeng Li[1,2], Jiakun Han[1,2], Thomas C. Ingalls[3,4], Jie Cheng[1,2], Yunjun Yao[1,2], Kun Jia[1,2], and Xiaotong Zhang[1,2]

[1]The State Key Laboratory of Remote Sensing Science, jointly sponsored by Beijing Normal University and Institute of Remote Sensing and Digital Earth of Chinese Academy of Sciences, Beijing, China.

[2]China and Beijing Engineering Research Center for Global Land Remote Sensing Products, Institute of Remote Sensing Science and Engineering, Faculty of Geographical Science, Beijing Normal University, Beijing, China.

[3]Center for Global Discovery and Conservation Science, Arizona State University, Tempe, AZ, 85281, USA.

[4]School of Earth and Space Exploration, Arizona State University, Tempe, AZ, 85281, USA.

Corresponding author: Bo Jiang(bojiang@bnu.edu.cn)

Abstract

The ocean-surface downward longwave radiation (R_l) is one of the most fundamental components of the radiative energy balance, and it has a remarkable influence on air–sea interactions. Because of various shortcomings and limits, a lot of empirical models were established for ocean-surface R_l estimation for practical applications. In this paper, based on comprehensive measurements collected from 65 moored buoys distributed across global seas from 1988 to 2019, a new model for estimating the all-sky ocean-surface R_l at both hourly and daily scales was built. The ocean-surface R_l was formulated as a nonlinear function of the screen-level air temperature, relative humidity, cloud fraction, total column cloud liquid, and ice water. A comprehensive evaluation of this new model relative to eight existing models was conducted under clear-sky and all-sky conditions at daytime/nighttime hourly and daily scales. The validation results showed that the accuracy of the newly constructed model is superior to other models, yielding overall RMSE values of 14.82 and 10.76 W/m^2 under clear-sky conditions, and 15.95 and 10.27 W/m^2 under all-sky conditions, at hourly and daily scales, respectively. Our analysis indicates that the effects of the total column cloud liquid and ice water on the ocean-surface R_l also need to be considered besides cloud cover. Overall, the newly developed model has strong potential to be widely used.

Keywords:Ocean surface, longwave radiation, empirical model, buoy

1 Introduction

The downward longwave radiation (R_l) at the ocean surface is the thermal infrared (4–100 μm) radiative flux emitted by the entire atmospheric column over the ocean surface (Yu et al., 2018).The ocean-surface R_l is among the most important components of the heat flux across the ocean–atmosphere interface, shaping the climate state of both the atmosphere and the ocean~~which, in turn, shapes the climate state of both the atmosphere and ocean~~ (Caniaux, 2005; Fasullo et al., 2009; Fung et al., 1984). Accurate estimates of R_l are essential for studying air–sea interactions and for improving our understanding of climate and oceanic systems. ~~Therefore, an accurate estimate of the ocean-surface R_l is crucial for studies of air–sea interactions and the climate and oceanic systems.~~

Although the ocean-surface R_l is ~~routinely~~ measured at most buoy sites, the available ocean-surface R_l measurements can not meet the needs of various applications because of the small number of buoys currently employed (especially moored buoys) and their sparse distribution across global oceans. Another way to get the R_l at the ocean surface is by using satellite-based or model reanalysis products. The ocean-surface R_l from satellite-derived products, such as the International Satellite Cloud Climatology Project (ISCCP) (Rossow & Zhang, 1995; Young et al., 2018) and Clouds and the Earth's Radiant Energy System Synoptic Radiative Fluxes and Clouds (CERES/SYN1deg) (Doelling et al., 2013; Rutan et al., 2015) is usually generated using these satellite data and a radiative transfer model, which simulates the radiative transfer interactions of light absorption, scattering, and emission through the atmosphere with the input of given atmospheric parameters. However, radiative transfer models are not widely used in practice because of their complexity ~~complicacy~~ and the difficulties associated with collecting all essential inputs. The ocean-surface R_l provided in model reanalysis products, such as the fifth generation of the European Centre for Medium-Range Weather Forecasts atmospheric reanalysis of the global climate (ERA5) (Hersbach et al., 2020) and the

58 Modern-Era Retrospective analysis for Research and Applications, Version 2 (MERRA2) (Gelaro
59 et al., 2017), is produced by assimilating various observations into an atmospheric model to get
60 the optimal estimates of the state of the atmosphere and the surface (Gelaro et al., 2017).
61 Previous studies indicated that R_l estimates from satellite-based products are generally in better
62 agreement with buoy measurements than those obtained from reanalysis products (Pinker et al.,
63 2014; Pinker et al., 2018; Thandlam & Rahaman, 2019). However, applications of the ocean-
64 surface R_l from these two kinds of products are limited due to their coarse spatial resolutions
65 (most of them are coarser than 1º), limited periods (especially satellite-based products) (Xu et al.,
66 2023; Zeng et al., 2020), and discrepancies in accuracy and consistency (Cronin et al., 2019).

67 To overcome these limitations,~~Hence~~, many parameterization and empirical models for
68 estimating ocean-surface R_l that can easily be implemented in practical use have been established
69 during the past few decades (Bignami et al., 1995; Josey, 2003; Zapadka et al., 2001). Most of
70 the commonly used R_l estimation models were established using the relationship between R_l and
71 the relevant meteorological variables (i.e., air temperature, humidity, column integrated water
72 vapor (IWV), and cloud parameters) or oceanic parameters (i.e., bulk sea surface temperature),
73 which are usually obtained from in situ measurements or model simulations (Li & Coimbra,
74 2019; Li et al., 2017; Paul, 2021). However, a significant limitation is that many of these models
75 were originally developed for land surfaces and applied directly to the ocean, assuming similar
76 atmospheric conditions. ~~It is known that most R_l estimation models were originally developed for~~
77 ~~the land surface and were applied to the ocean surface directly without any alterations by~~
78 ~~assuming the atmospheric conditions are nearly the same over ocean and land surfaces~~ (Bignami
79 et al., 1995; Clark et al., 1974; Frouin et al., 1988; Josey, 2003). This assumption introduces the
80 uncertainty in R_l estimates, as water vapor profiles differ significantly between land and ocean
81 surfaces~~However, this assumption increases the uncertainty in R_l estimates because of the~~
82 ~~significantly different water vapor profiles over ocean and land surfaces~~ (Bignami et al., 1995).
83 Even those models specifically designed for ocean surfaces are often based on limited regional
84 data, raising concerns about their robustness when applied globally.~~A few models built~~
85 ~~specifically for R_l estimation at the ocean surface~~ (Bignami et al., 1995; Josey, 2003; Zapadka et
86 al., 2001) ~~were usually developed using limited observations collected from buoy sites or cruise~~
87 ~~ships distributed within a specific region; hence, the robustness of these models were in doubt~~
88 ~~when applied globally~~. For example, Josey (2003) proposed a model for R_l estimation at mid-to-
89 high latitude seas with a satisfactory validation accuracy, but this new model performed worse
90 over tropical seas with a tendency to underestimate R_l by up to 10–15 W/m^2.
91 Furthermore~~Moreover~~, most of the existing R_l estimation models only work under clear-sky
92 conditions, which are especially rare over ocean surfaces. Additionally~~Furthermore~~, most of
93 these models only derive R_l at instantaneous scales, yet the R_l at the daily scale is more preferred
94 across a range of applications.

95 Given these challenges, there is a clear need for a new, easily implemented model capable
96 of providing accurate R_l estimates at the global ocean surface. Such a model should function
97 effectively under all-sky conditions, offer flexibility in temporal scales (e.g., instantaneous and
98 daily), and be robust enough for global application. Addressing these gaps would provide a
99 valuable tool for improving our understanding of air–sea interactions and contribute to more
100 accurate climate and oceanic models. More details about the existing R_l estimation models are
101 given in Section 2.

102 ~~Therefore, a new, easily implemented model that can derive accurate and robust R_l~~

106   In addition, according to W Wang and Liang (2009b), the uncertainty of the ocean-surface
107 R_l estimation should be less than 10 W/m^2 for climate diagnostic studies. However, the
108 performances of the most commonly used R_l estimation models at the global ocean surface were
109 not thoroughly evaluated in previous studies because of the few available in situ measurements.
110 Fortunately, being aware of the significance of the energy budget in air–sea interactions
111 (Centurioni et al., 2019), more and more platforms for radiative measuring have been built across
112 global ocean surfaces during the past decades, so relatively comprehensive ocean-surface R_l
113 measurements can be collected today, which provide a good opportunity for modeling and
114 comprehensive evaluations.

115   Overall, the main goal of this research is to establish a new empirical model for
116 calculating the all-sky ocean-surface R_l at instantaneous and daily scales based on globally
117 distributed moored buoy measurements and other ancillary information. A comprehensive
118 evaluation is conducted on the newly developed model relative to eight commonly used models
119 for ocean-surface R_l estimation under clear- and all-sky conditions at hourly and daily scales.
120 The organization of this paper is as follows. A review of the eight commonly used R_l estimation
121 models is presented in Section 2. Section 3 introduces the data sets used in this research and the
122 methods, including the new model development and model evaluation. Section 4 shows the
123 results of the model validation, comparison, and analysis. The key conclusions and discussions
124 are provided in Section 5.

125   2 Review of Previous Models

126   Many models were proposed for R_l calculation under various sky conditions at different
127 temporal scales in previous studies. In this study, eight widely used models were selected for
128 evaluation and Table 1 shows their basic information. According to the sky conditions under
129 which these models could be used, the eight R_l estimation models were divided into two classes:
130 R_l models under clear-sky conditions and under all-sky conditions, respectively. Details of the
131 eight models are provided one by one in the following section. Note that the downward direction
132 is defined as positive in this study.

133 **Table 1**

134 *Eight Existing Models for Ocean-surface R_l Estimation, with Variables Explained in Table 2.*

Sky Condition	Model	Abbr	Designed temporal scale	Reference
	$R_l = a\sigma T_a^4(1+b\sqrt{e})$	Mod1	Monthly	Brunt (1932)
	$R_l = \sigma T_a^4\{1-a\exp(-b(273-T_a)^2)\}$	Mod2	5–15 minute	Idso and Jackson (1969)
Clear-sky	$R_l = a\sigma T_a^4(e/T_a)^{1/7}$	Mod3	Instantaneous	Brutsaert (1975)
	$R_l = a\sigma T_a^4[1-\exp(-e^{T_a/2016})]$	Mod4	Daily	Satterlund (1979)
	$R_l = \sigma T_a^4[1-(1+\varepsilon)\exp\{-(1.2+3\varepsilon)^{1/2}\}]$	Mod5	Instantaneous	Prata

	$\varepsilon=46.5(\dfrac{e}{T_a})$			(1996)
All-sky	$R_l=\dfrac{\varepsilon\sigma T_s^4-\varepsilon\sigma T_s^4\left(a+b\sqrt{e}\right)\left(1-\lambda C^2\right)+4\varepsilon\sigma T_s^3(T_s-T_a)}{1-\alpha_l}$	Mod6	Daily	Clark et al. (1974)
	$R_l=\sigma T_a^4(a+be)(1+dC^2)$	Mod7	Hourly	Bignami et al. (1995)
	$R_l=\sigma\{T_a+aC^2+bC-d+g(D+f)\}^4$	Mod8	Hourly	Josey (2003)

135   2.1 Under clear-sky condition

136   Among the eight models, there are five R_l estimation models that could only be used
137 under clear-sky conditions.

138   Brunt (1932) developed the first R_l estimation model (named Mod1) for land surfaces,
139 which relates the monthly mean R_l to the screen-level water vapor and air temperature, as
140 Equation (1) shows:

141 $$R_l=a_1\sigma T_a^4(1+b_1\sqrt{e}) \tag{1}$$

142   where a_1 and b_1 are empirical coefficients, T_a is the monthly mean screen-level air
143 temperature (K), e is the monthly mean screen-level water vapor pressure (mbar), and σ is the
144 Stefan–Boltzmann constant, defined as $5.67\times10^{-8}\,\text{W}/(\text{m}^2\cdot\text{K}^4)$. In the study of Brunt (1932), the
145 two coefficients a_1 and b_1 were suggested as 0.52 and 0.125 based on observations collected from
146 Benson, South Oxfordshire, England. The validation results of Mod1 showed a correlation
147 coefficient as high as 0.97 based on the collected samples. However, Swinbank (1963) pointed
148 out that the validation results of Mod1 for other regions where variations in the humidity and T_a
149 were different from those in Benson were worse. Despite these limitations, as the first empirical
150 R_l estimation model in a simple format, Mod1 has been widely used to construct the coupling
151 between hydrological and atmospheric models (Habets et al., 1999; Lohmann et al., 1998).

152   Different from Mod1, the model developed by Idso and Jackson (1969) (named Mod2)
153 was based on the theoretical consideration that the effective emittance of an atmosphere is solely
154 temperature-dependent; hence, the screen-level T_a is the only input of Mod2 for calculating R_l:

155 $$R_l=\sigma T_a^4\{1-a_2\exp(-b_2(273-T_a)^2)\} \tag{2}$$

156   where a_2 and b_2 are empirical coefficients, which were defined as 0.261 and 7.770×10^{-4},
157 respectively, by Idso and Jackson (1969) based on experimental data at four sites located in
158 Arizona, Alaska, Australia, and the Indian Ocean, obtained at intervals of 5 to 15 minutes. Idso
159 and Jackson (1969) thought that Mod2 might be efficient at all latitudes for different seasons, as
160 it has been developed by using observations from diverse locations. Since publication, Mod2 has
161 been employed in relevant researches like evaporation estimation (Cleugh et al., 2007; Vertessy
162 et al., 1993) and ocean-ice modeling (Saucier et al., 2003).

163   Afterwards, Brutsaert (1975) proposed a simple model for computing R_l by directly
164 solving the Schwarzschild's transfer equation (Schwarzschild, 1914) under clear skies and
165 standard atmospheric conditions (i.e., the U.S. 1962 standard atmosphere). This model is denoted
166 as Mod3, and is described as follows:

167 $$R_l=a_3\sigma T_a^4(e/T_a)^{1/7} \tag{3}$$

168   where a_3 is defined as a constant equal to 1.24, as determined during the Schwarzschild's
169   transfer equation solving process. Explicit physical theory is reflected in Mod3. The term
170    $(e/T_a)^{1/7}$, regarded as the atmospheric emissivity, tends to zero when the water vapor content is
171   very little. However, Prata (1996) indicated that the atmospheric emissivity tends to a certain
172   constant value even without water vapor, such as values from 0.17 to 0.19 when only CO_2 is
173   present (Staley & Jurica, 1972). The estimates from Mod3 are usually used as the necessary
174   inputs of hydrological models (Pauwels et al., 2007; Rigon et al., 2006) and climate models
175   (Mills, 1997).

176   Aase and Idso (1978) found that Mod2 and Mod3 performed poor when T_a was below
177   freezing. To address this issue, Satterlund (1979) proposed a model (named Mod4) to compute R_l
178   by reformatting T_a and e, as follows:

$$R_l=a_4\sigma T_a^4\left[1\text{-}\exp(\text{-}e^{T_a/2016})\right] \tag{4}$$

180   where a_4 is an empirical coefficient and defined as 1.08 by Satterlund (1979) based on
181   collected daily R_l measurements at one site in Sidney, Montana, USA. After validation and
182   comparison, Satterlund (1979) concluded that Mod4 outperformed Mod2 and Mod3 under
183   extreme conditions in terms of temperature and humidity and performed comparably with the
184   two models for other cases. As such, the R_l estimates from Mod4 have been used in studies such
185   as snow pack evolution (Douville et al., 1995) and hydrological models (Schlosser et al., 1997).
186   However, because the model does not contain a constant term, the application of Mod4 should be
187   done with caution if the surface water vapor pressure is very close to zero.

188   With the development of radiation measuring instruments and technology, several new R_l
189   estimation models have been proposed, such as the model proposed by Prata (1996) (named
190   Mod5), as follows:

$$R_l=\sigma T_a^4\left[1\text{-}(1+46.5(\tfrac{e}{T_a}))\exp\left\{\text{-}\left(a_5+46.5b_5(\tfrac{e}{T_a})\right)^{1/2}\right\}\right] \tag{5}$$

192   where a_5 and b_5 are empirical coefficients, defined as 1.2 and 3.0 in the study of Prata
193   (1996) and Robinson (1947; 1950). As with Mod1–Mod4, Mod5 is also dependent on T_a and e
194   but contains a majorly revised right term (in the square brackets), which is regarded as the
195   emissivity. After extensive validation and comparison, Prata (1996) claimed Mod5 outperformed
196   or performed similar to other R_l estimation models, including Mod1–Mod4, in areas within the
197   polar region, mid-latitudes, and tropical regions. Hence, Mod5 has been applied widely, from
198   studies of snowmelt modeling (Jost et al., 2009) to urban energy budget (Nice et al., 2018;
199   Oleson et al., 2008).

200   To sum up, all five R_l estimation models (Mod1–Mod5) that only work under clear-sky
201   conditions take T_a and/or e as inputs. Such an approach is in agreement with the research of
202   Kjaersgaard et al. (2007) who found that R_l is mainly emanated from the low-level atmosphere
203   that can be adequately characterized in terms of T_a and humidity under clear-sky conditions
204   (Diak et al., 2000; Ellingson, 1995; Prata, 1996). Moreover, the five models were all established
205   by using measurements from different regions at various timescales, and they can be employed at
206   any timescale (see Table 1) regardless of the temporal resolution of the original measurements
207   used for modeling.

208   2.2 Under all-sky condition

209   Three R_l estimation models that can work under all-sky conditions were evaluated in this
210 paper. Comparing to the above five models, ancillary information (e.g., clouds) should be taken
211 into account in addition to T_a and e in the three models, and the three models were developed
212 specifically for ocean surfaces.

213   Based on the model developed by Clark et al. (1974) for the all-sky net longwave
214 radiation at the ocean surface (R_{lnet}, the difference between the downward and upward longwave
215 radiation) calculation, Josey (2003) proposed a revised model (named Mod6) to estimate the all-
216 sky ocean-surface R_l by getting rid of the ocean-surface upward longwave radiation as:

217
$$R_l = \frac{\varepsilon_s \sigma SST^4 - \varepsilon_s \sigma SST^4 \left(a_6 + b_6 \sqrt{e}\right)\left(1 - \lambda C^2\right) - 4\varepsilon_s \sigma SST^3 (SST - T_a)}{1 - \alpha_s} \tag{6}$$

218   where ε_s is the sea surface emissivity, defined as a constant value of 0.98, and SST is the
219 sea surface temperature (K); hence, the term $\varepsilon_s \sigma SST^4$ is the upward longwave radiation at the
220 ocean surface. α_s is the sea surface longwave radiation reflectivity, defined as a constant value of
221 0.045, C is the cloud cover (0–1; dimensionless), λ is a latitude-dependent coefficient that
222 represents the cloud amount, and a_6 and b_6 are empirical coefficients. Based on measurements
223 (i.e., R_l, T_s, and C) collected from the Chemical and Hydrographic Atlantic Ocean Section
224 (CHAOS) in the northeast Atlantic in 1998, a_6 and b_6 were determined as 0.39 and -0.05 (Clark et
225 al., 1974; Josey, 2003), and λ at a given latitude can be taken from Josey et al. (1997). Josey
226 (2003) validated Mod6 and the results showed that Mod6 tended to overestimate the
227 instantaneous R_l measurements from CHAOS by 11.70 W/m^2. The estimates from Mod6 have
228 been applied in hydrodynamic models (Grayek et al., 2011) and atmospheric boundary layer
229 models (Deremble et al., 2013).

230   Based on hourly cruise measurements (i.e., R_l, T_a, and C) collected in the Mediterranean
231 Sea during the period from 1989 to 1992, Bignami et al. (1995) proposed an empirical model to
232 calculate the ocean-surface all-sky R_l (named Mod7) as follows:

233
$$R_l = \sigma T_a^4 (a_7 + b_7 e)(1 + c_7 C^2) \tag{7}$$

234   where a_7, b_7, and c_7 are empirical coefficients defined as 0.684, 0.0056, and 0.1762,
235 respectively. Bignami et al. (1995) presented validated RMSE values for Mod7 which ranged
236 from ~14 W/m^2 at the hourly scale to ~9 W/m^2 at the daily scale. Mod7 has been utilized by the
237 Mediterranean Forecasting System for predictions of currents and biochemical parameters
238 (Pinardi et al., 2003), coupled ocean–atmosphere climate models (Dubois et al., 2012) as well as
239 generation of the Atlantic Ocean heat flux climatology (Lindau, 2012).

240   Also based on the measurements collected from CHAOS, Josey (2003) assessed the
241 accuracy of Mod7 and found that this model tended to underestimate the all-sky R_l by 12.10
242 W/m^2 at the instantaneous scale. After analyzing the shortcomings of Mod6 and Mod7, Josey
243 (2003) proposed a new model (named Mod8) for all-sky ocean-surface R_l calculation through a
244 revision of T_a by using the same samples:

245
$$R_l = \sigma \left\{ T_a + a_8 C^2 + b_8 C - c_8 + d_1 (D + e_1) \right\}^4 \tag{8}$$

246   where a_8, b_8, c_8, d_1, and e_1 are empirical coefficients determined as 10.77, 2.34, 18.44,

247 0.84, and 4.01, respectively, D is the dew point depression, and T_a is the temperature (K) (see
248 Equation (11)). Estimates of R_l obtained with Mod8 agreed to within 2 W/m^2 in the mean bias of
249 10 minute measurements at middle-high latitudes. The estimates from Mod8 have been used as
250 essential input in simulations of ocean–atmosphere interactions in the Arctic shelf (Cottier et al.,
251 2007).

252   Overall, it was thought that variations in the all-sky ocean-surface R_l were related to T_a, e,
253 and cloud information (e.g., cloud cover and cloud amount) in previous studies. However, Fung
254 et al. (1984) pointed out that other relevant cloud information, such as the cloud base height
255 (CBH) and cloud optical thickness, also have a significant influence on ocean-surface longwave
256 radiation. Therefore, more efforts should be made to increase the R_l estimation accuracy under
257 all-sky conditions.

258 **3 Data and Methodology**

259   In order to develop a new all-sky ocean-surface R_l estimation model, the meteorological
260 and radiative observations from 65 moored buoys and the cloud parameters from the ERA5
261 reanalysis product from 1988 to 2019 were applied. Afterwards, the newly developed model and
262 the eight commonly used models (Mod1–Mod8) were evaluated against the moored R_l
263 measurements under clear- and all-sky conditions at hourly/daily scales

264   3.1 Data and pre-processing

265   Table 2 lists all the variables employed in this paper and their information. The
266 instantaneous timescale can be defined as timescales ranging from a 3 minute average to hourly
267 average (Bignami et al. (1995); K Wang and Liang (2009a); hence, two timescales, hourly and
268 daily, were considered in this study for model evaluation as in previous studies (Bilbao & de
269 Miguel, 2007; Kjaersgaard et al., 2007; Sridhar & Elliott, 2002). Note that Mod1 was also used
270 at the two timescales (Guo et al., 2019) though it was originally established with monthly
271 samples. More details about the data are given below.

272 **Table 2**
273 *Variables: Explanations and Sources*

Abbreviation	Full name	Time scales	Unit	Source
RH	Relative humidity	Daily/hourly	%	In situ
e	Water vapor	Daily/hourly	hPa	Calculated
T_a	2-m air temperature	Daily/hourly	K	In situ
T_s	Sea surface temperature	Daily/hourly	K	In situ
D	Dew point depression	Daily/hourly	K	Calculated
CI	Clearness index	Daily/hourly	0-1	Calculated
C	Fractional cloud cover	Daily/hourly	0-1	Calculated
clw	Total column cloud liquid water	Daily/hourly	g/m^2	ERA5
ciw	Total column cloud ice water	Daily/hourly	g/m^2	ERA5
R_l	Downward longwave radiation	Daily/hourly	W/m^2	In situ
R_g	Downward shortwave radiation	Daily/hourly	W/m^2	In situ
DSR_{toa}	Extraterrestrial solar radiation (DSR_{toa})	Daily/hourly	W/m^2	Modeled

274   3.1.1 Measurements from moored buoys

275   All measurements were collected from 65 moored buoy sites, whose latitudes range from
276 47°S to 59.5°N, as shown in Figure 1. The majority of moored buoy sites were located in
277 tropical seas (23.5°S–23.5°N), and relatively few buoys were in the high-latitude seas of the
278 Northern Hemisphere (>50°N) and the mid-high latitude seas of the Southern Hemisphere
279 (>30°S).
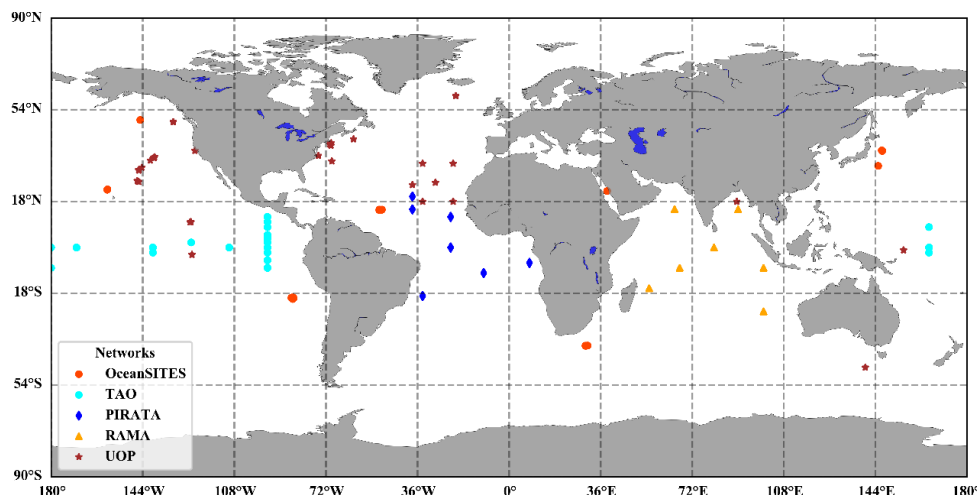
281 **Figure 1.** Spatial distribution of the 65 moored buoys.

282   The moored buoy sites in this study belong to five well-known observation
283 network/programs, including the Upper Ocean Processes Group (UOP), Tropical Atmosphere
284 Ocean/Triangle Trans-Ocean Buoy Network (TAO/TRITON), Pilot Research Moored Array in
285 the Tropical Atlantic (PIRATA), Research Moored Array for African–Asian–Australian Monsoon
286 Analysis and Prediction (RAMA), and OceanSITES. Launched by the Woods Hole
287 Oceanographic Institution (WHOI), UOP mainly focuses on studying the physical processes of
288 the air-sea interface and the epipelagic, and its buoys are equipped with oceanographic and
289 meteorological sensors. The UOP measurements accurately quantify annual cycles of wind stress
290 and net air-sea heat exchange in the Southern Ocean (Schulz et al., 2012). Twenty-two sites form
291 the UOP, and data from all were used in this study. TAO/TRITON (McPhaden et al., 1998) in the
292 tropical Pacific, PIRATA (Bourlès et al., 2008) in the tropical Atlantic, and RAMA in the tropical
293 Indian Ocean (McPhaden et al., 2009) are all part of the Global Tropical Moored Buoy Array
294 (GTMBA) program (McPhaden et al., 2010). Extensive quality control was done by GTMBA
295 prior to dissemination of the data (Freitag, 1999; 2001; Lake, 2003; Medovaya et al., 2002), and
296 they have been used for monitoring, understanding, and forecasting the El Niño–Southern
297 Oscillation (ENSO) and monsoon variability (McPhaden et al., 2009). Data from 35 GTMBA
298 sites (TAO, 21; PIRATA, 7; RAMA, 7) were used in this study. The OceanSITES network is
299 composed of buoys funded by oceanographic researchers across the globe. The goal of the
300 OceanSITES program is to facilitate the use of high-quality multidisciplinary data from fixed
301 sites in the open ocean (Cronin et al., 2019). Eight sites from OceanSITES were utilized,
302 specifically: OS_PAPA, OS_KAUST, OS_NTAS, OS_KEO, OS_ARC, OS_JKEO,
303 OS_STRATUS, and OS_WHOTS. In this study, the routine measurements made at moored
304 buoys, including radiative measurements (e.g., ocean-surface downward shortwave radiation R_g)
305 and meteorological measurements (e.g., T_a and RH) were collected and used; other variables
306 (e.g., e, D, and CI) were calculated from these measurements. More information regarding these

307   data sets is found in Table 3.

308   **Table 3**

309   *Descriptions of Different Networks*

Network/Program	No. of sites	Period	Observation frequency	Variables	URL
UOP	22	1988-2017	1 hour	R_l, R_g, T_a,RH	http://uop.whoi.edu/index.html
TAO/TRITON	21	2000-2019	10 min	R_l, R_g, T_a,RH	https://www.pmel.noaa.gov/tao/drupal/disdel/
RAMA	7	2004-2019	10 min	R_l, R_g, T_a,RH	https://www.pmel.noaa.gov/tao/drupal/disdel/
PIRATA	7	2006-2019	10 min	R_l, R_g, T_a,RH	https://www.pmel.noaa.gov/tao/drupal/disdel/
OceanSITES	8	2000-2018	1 hour	R_l, R_g, T_a,RH	http://www.oceansites.org/

310   3.1.1.1 Radiative measurements

311   At each moored buoy, R_l is routinely measured by an Eppley Precision Infrared
312   Radiometer (PIR) with a nominal accuracy of ±1% (Richard E. Payne & Anderson, 1999), and
313   R_g is routinely measured by an Eppley Laboratory precision spectral pyranometer (PSP) with a
314   calibration accuracy of ±2% (Freitag, 1994). The PIR and PSP are deployed approximately 3 m
315   above sea level. All measurements are quality controlled by their providers. To ensure data
316   quality, a two step approach was implemented; 1) only observations flagged as 'high quality' by
317   the data providers were considered, and 2) data was manually inspected by the authors for any
318   irregularities. Additionally, the R_l measurements above 450 W/m^2 were removed, as suggested
319   by Josey (2003).

320   As pointed out by Pascal and Josey (2000), the main errors in measuring R_l are from the
321   shortwave leakage and differential heating of the sensor. Therefore, the errors (ΔR_l) in R_l
322   observations were corrected according to Pascal and Josey (2000) as:

323
$$\Delta R_l=(a+\lambda)R_g+bR_g^2 \tag{9}$$

324   where a = 4.34×10^{-3}, λ = 0.011, and b = 1.72×10^{-6}. The differences between λ = 0.007,
325   0.011, and 0.024 resulted in minimal changes to R_l, with 78% and 72% of samples showing
326   deviations of less than 1 W/m² and 4 W/m², respectively. These values are below the sensors'
327   uncertainty. Therefore, we used 0.011 for λ. Hence, the R_l measurements at a sampling frequency
328   less than one hour were first corrected. After that, selected measurements whose sampling
329   frequency was less than one hour were aggregated into hourly means as long as 80% of the
330   measurements in one hour were available, and the hourly data were aggregated into daily means
331   as long as 24 hourly data in one day were available.

332   Note that the errors of the measured R_g induced by buoy rocking motions, sensor tilting,
333   and aerosol accumulation (Medovaya et al., 2002) were too small to be considered here. At lastIn
334   total, 47,266 samples at the daily scale and 1,275,308 samples at the hourly scale during the
335   period from 1988 to 2019 were used in this study. For better comparison, the hourly samples
336   used for independent validation were further divided into daytime (R_g > 120 W/m^2) and
337   nighttime conditions (R_g ≤ 120 W/m^2), with 147,981 samples in daytime and 210,057 in
338   nighttime.

339   3.1.1.2 Meteorological and oceanic variables

340   Two meteorological measurements, RH and T_a, were collected at the moored buoy sites.
341 The instrument used for measuring RH and T_a is a Rotronic MP-100F, deployed about 3 m above
342 the sea level. The instrument produced accuracies of 2.7% and 0.2 K (Lake, 2003) for RH and
343 T_a, respectively, which are also too small to influence the accuracy of the R_l estimation. Similar
344 to the radiative measurements, RH and T_a were both strictly screened and then aggregated into
345 hourly and daily means.

346   ~~On the contrary~~On the other hand, the sea surface temperature (SST) was measured at
347 about 1 m below the sea level using a high-accuracy conductivity and temperature recorder
348 (SBE37/39; Sea Bird Electronics) with an accuracy of 0.002 K. According to Donlon et al.
349 (2002), there is a strong correlation between body SST and skin SST. Although wind speed has a
350 significant effect on this relationship, a constant correction offset can be applied when the wind
351 speed exceeds 6 m/s (Alappattu et al., 2017). In fact, 83% of the samples had wind speeds above
352 4 m/s, and as suggested by Vanhellemont (2020), the bulk SST measured at moored buoys can be
353 adjusted to the skin SST by using a correction offset of 0.17 K.

354   3.1.1.3 *Calculation of other variables*

355   Three variables, including e, D, and CI, were calculated with the RH, T_a, and R_g,
356 measurements separately. Therefore, these three variables at hourly and daily scales were
357 obtained from the corresponding measurements. Specifically, the daily (hourly) mean e was
358 calculated from the daily (hourly) RH using the following equation:

359
$$e=6.1121 \frac{RH}{100} \exp(\frac{17.502 T_a}{T_a+240.97}) \tag{10}$$

360   Note that Equation (10) only works when T_a is in the range -30–50 °C (Buck, 1981), and
361 T_a should be in items of °C.

362   The daily (hourly) dew point depression D was calculated according to Josey (2003) and
363 Henderson-Sellers (1984) as:

364
$$D= 34.07+4157/\ln(2.1718*10^8/e) - T_a \tag{11}$$

365   The clearness index (CI) is calculated as the ratio of the surface R_g to the extraterrestrial
366 solar radiation (DSR_{toa}) (Ogunjobi & Kim, 2004). CI generally represents the atmospheric
367 transmissivity affected by permanent gases, aerosols, and the optical thickness of the clouds
368 (Alados et al., 2012; Flerchinger et al., 2009; Gubler et al., 2012; Jiang et al., 2015; Meyers &
369 Dale, 1983), and it is widely used in radiation related researches (Iziomon et al., 2003; Jiang et
370 al., 2016; Jiang et al., 2015; Richard E Payne, 1972). The value of CI is between 0 and 1, where a
371 larger CI value represents a clearer sky. The hourly CI can be calculated as follows:

372
$$CI = \frac{R_g}{DSR_{toa}} \tag{12}$$

373   However, during nighttime, the hourly CI cannot be calculated by Equation (12) directly
374 because of a lack of R_g values; hence, it was calculated based on a 24-hour solar radiation
375 window centered on the hourly observation as suggested by Flerchinger et al. (2009). The daily
376 CI was calculated as the average of all hourly CI values in a day for the sake of considering
377 atmosphere variations at nighttime.

In this paper, CI was utilized to determine the condition as clear-sky when its value was greater than 0.7 at both hourly and daily scales. Additionally, it was found that the cloud cover derived from CI would help to improve the model performance after multiple experiments, especially at nighttime. Therefore, CI was also used to calculate the cloud cover. Specifically, the cloud fraction was linearly interpolated between C = 1.0 at a CI value of 0.4 for complete cloud cover to C = 0.0 at a CI value of 0.7 for cloudless, both at daily and hourly scales according to Flerchinger et al. (2009). Because of the different calculation of CI during daytime and nighttime, the uncertainty in the calculated cloud cover was different; hence, the R_l estimates at the hourly scale were further examined at daytime and nighttime. Therefore, all meteorological factors (RH, T_a, e, and D) at daily and at hourly scales were respectively prepared accordingly.

3.1.2 Cloud parameters from the ERA5 reanalysis data set

As described above, the cloud cover represented by the fraction (C) is usually taken into account when estimating R_l affected by clouds. However, in this study, two more cloud-related parameters, including clw and ciw (see Table 2̶1̶), from the ERA5 reanalysis product were also considered in the modeling. The total amount of liquid water per unit area in the air column from the base to the top of the cloud is called the total column cloud liquid water (clw), and its chilled counterpart (ice) is called the total column cloud ice water (ciw) (Nandan et al., 2022). ERA5 is the fifth generation atmospheric reanalysis product, and it was produced based on 4D-Var data assimilation using the Integrated Forecasting System (IFS) with an enhanced spatial resolution (0.25°) and time resolution (hourly) compared to its previous version ERA-interim (Hoffmann et al., 2019) from 1979 to present. Clouds in ERA5 are represented by a fully prognostic cloud scheme, in which cloud fractions and cloud condensates obey mass balance equations (Tiedtke, 1993). The ERA5 clw values are in good agreement with those obtained from radiosonde observations (Nandan et al., 2022). Overall, relative to ERA-interim, ERA5 shows reduced biases in the total ice water path versus other satellite-based observational products. Therefore, the two cloud parameters were extracted from the locations of the 65 moored buoy sites directly at the hourly scale, and then their daily means were calculated by averaging the 24 valid hourly values. ERA5 cloud product is available on the Climate Data Store (CDS) cloud server (https://cds.climate.copernicus.eu/cdsapp#!/search?type=dataset).

Overall, 70% of the samples at each moored buoy site, including 33,151 daily samples and 917,270 hourly samples, were randomly selected for new model training and calibration of the eight previous models (Mod1– Mod8). The other 30% of the data at each site, including 14,115 daily samples and 358,038 hourly samples (daytime: 147,981; nighttime: 210,057), were used for model validation.

3.2. Methodology

A new model that could estimate ocean-surface R_l under all-sky conditions at both hourly and daily scales was developed based on the moored measurements and ERA5 cloud parameters. Moreover, the eight evaluated R_l models were all recalibrated so as to evaluate the model's accuracy objectively. Based on the corresponding validation samples, the R_l values produced by the nine models were compared under clear-sky and all-sky conditions at hourly and daily scales, where the comparison at the hourly scale was further divided into daytime and nighttime values.

419   3.2.1 New R_l estimation model development

420   As mentioned above, T_a and the humidity-related factors (e.g., RH) were enough to
421   characterize the variations in R_l under clear-sky conditions. However, for cloudy skies, R_l is
422   enhanced by the cloud base emitting (T Wang et al., 2020; Yang & Cheng, 2020). Cloud cover is
423   one of the most commonly used cloud-related parameters. In addition, theoretically, the cloudy-
424   sky R_l is significantly influenced by the cloud's base temperature, which is determined by the
425   CBH; hence, CBH is thought to be necessary in determining R_l under cloudy-sky conditions
426   (Viúdez-Mora et al., 2015). However, it is difficult to obtain the CBH accurately, especially for
427   partly cloudy skies (Zhou & Cess, 2001) because of the unavailability of the cloud's geometrical
428   thickness (Yang & Cheng, 2020). Therefore, other parameters that could provide information on
429   the CBH were explored. In the study of Hack (1998), a physical correlation between clw and
430   CBH was revealed for most cases, while clw was successfully used as an effective surrogate of
431   the CBH in the study of Zhou and Cess (2001). However, Zhou et al. (2007) pointed out that the
432   effects of ice clouds on R_l should also be considered when the atmospheric water vapor is low or
433   at high latitudes, which means that ciw also needs to be taken into account. Inspired by these
434   studies, clw and ciw, both in logarithmic form, were introduced in the development of a new
435   model named Modnew, in which R_l under all-sky conditions at the ocean surface was related to
436   five parameters including T_a, RH, clw, ciw, and C. Modnew was trained by the corresponding
437   training samples at hourly and daily scales. Details of the development of the new model
438   presented in the present study are given in Section 4.1.

439   3.2.2 Model performances evaluation

440   Table 4 lists the different cases for the R_l model comparison. As shown in Table 4, the
441   nine evaluated models (Mod1–Mod8 and Modnew) were all used for clear-sky R_l estimation at
442   both hourly and daily scales, while only four models (Mod6–Mod8 and Modnew) were evaluated
443   under all-sky conditions. Three metrics were employed to present the model accuracy: R^2, the
444   root-mean-square error (RMSE), and bias. Generally, all three statistics were calculated to
445   evaluate the accuracy of different models, but the RMSE values had larger weights.

446   **Table 4**
447   *Detailed Information of the Six Cases Considered in the Model Evaluation*

Case			Training samples	Validation samples	Evaluated model
Clear-sky	Hourly	Daytime	176,510	40,805	Mod1-Mod8, Modnew
		Nighttime		35,125	Mod1-Mod8, Modnew
	Daily		3,443	1,447	Mod1-Mod8, Modnew
All-sky	Hourly	Daytime	917,270	147,981	Mod6-8, Modnew
		Nighttime		210,057	Mod6-8, Modnew
	Daily		33,151	14,115	Mod6-8, Modnew

448   **4 Results and Analysis**

449   In this section, Modnew is introduced first, and then the validation results of the nine
450   evaluated models under various cases are compared and analyzed. Lastly, further analyses are
451   conducted on Modnew.

452   4.1 Modnew development

453   As mentioned above, the ocean-surface R_l in Modnew is related to five parameters (T_a,
454 clw, RH, C, and ciw) for hourly and daily scales under all-sky conditions. To understand better
455 the contribution made by each variable on R_l, the five parameters were introduced into Modnew
456 gradually. Taking the daily all-sky R_l as an example, R_l was first only characterized by the fourth
457 power of T_a based on the Stefan–Boltzmann law as follows:

458
$$R_l = a_{new}\sigma T_a^4 + b_{new} \tag{13}$$

459   where a_{new} and b_{new} are empirical coefficients, determined as 0.85 and 14.96, respectively,
460 based on the daily training samples. Then, the correlations between the model residuals in R_l
461 (referred to as ΔR_l) that define the difference between the in situ R_l measurements and the R_l
462 estimates from Equation (13) and other four parameters (clw, RH, C, and ciw) were explored one
463 by one. The results are found in Figure 2.

464
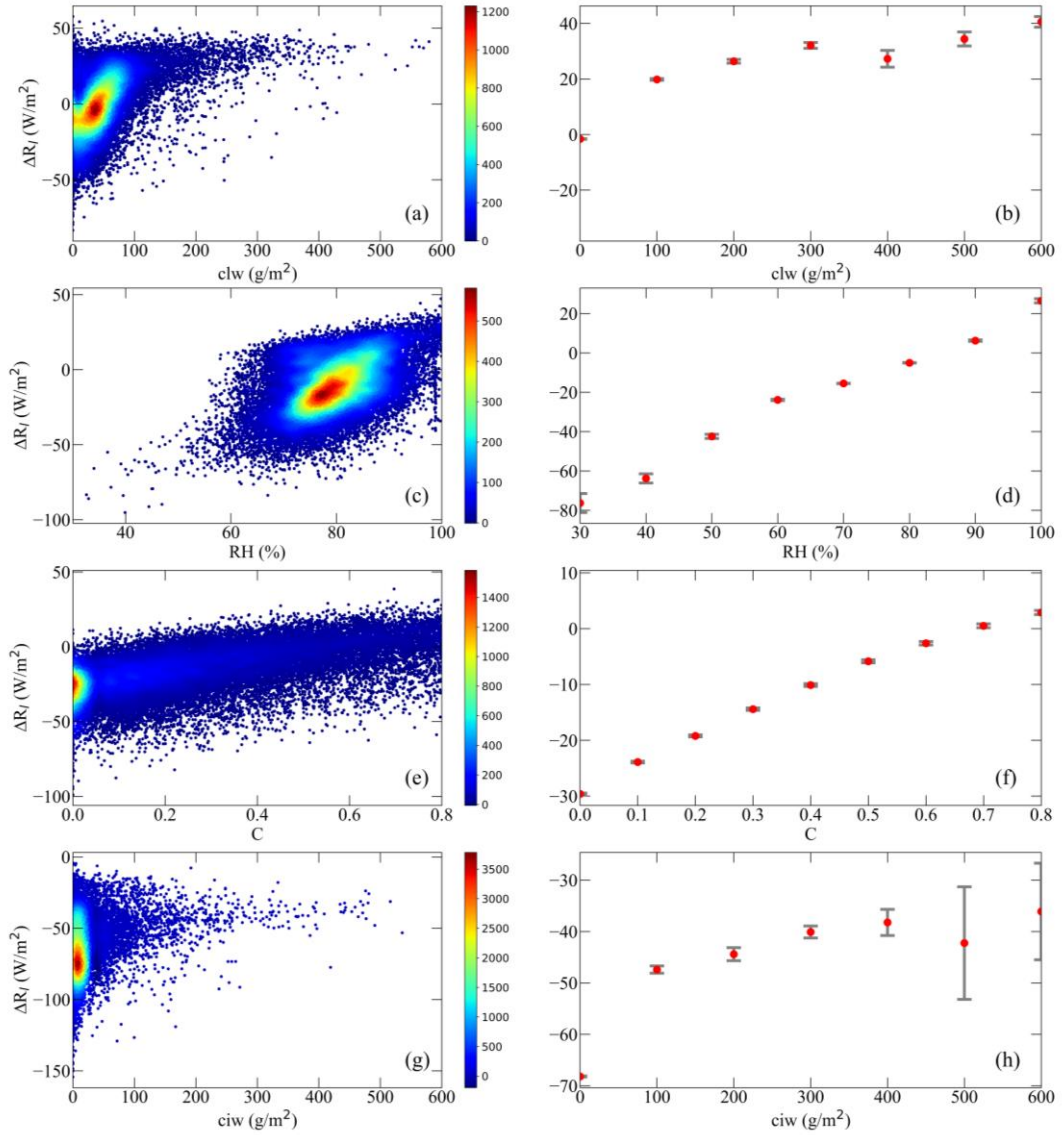
Figure 2. The scatter plots between the model residuals, ΔR_l, from Equation (13) and (a) clw, (c) RH, (e) C, and (g) ciw. Panels (b), (d), (f), and (h) are their corresponding box plots. In the left column, the color bar represents points per unit area. In the right column, the dots indicate the mean value of the ΔR_l (ME), while the vertical lines represent the standard error of the mean (SEM).

Figures 2(a), 2(c), 2(e), and 2(g) present scatter plots between ΔR_l and clw, RH, C, and ciw, respectively. In order to show their relationships better, the corresponding box plots, in which the mean of ΔR_l and its standard error (SEM) for each bin of the four parameters (in 10% increments) were calculated and presented in Figures 2(b), 2(d), 2(f), and 2(h), respectively. Specifically, ΔR_l varied with clw and ciw in a logarithmic relationship (Figures 2(b) and 2(h), respectively), and with RH (Figure 2(d)) and C (Figure 2(f)) in approximately linear relationships. Wefound that by introducing the C, RH, clw and ciw in Equation (13) gradually, the RMSE error was reduced from 17.48 W/m^2 with Equation (13) to 12.61 W/m^2, 10.92 W/m^2, 10.11 W/m^2 and 9.87 W/m^2, and the level of R^2 increased accordingly from 0.64 to 0.81, 0.86, 0.88 and 0.89, respectively. Hence, clw, RH, C, and ciw were introduced into Equation (13) in their appropriate forms and the final equation was taken as Modnew:

$$R_l = a_{new}\sigma T_a^4 + b_{new}C + c_{new}\ln(1+clw) + d_{new}\ln(1+ciw) + e_{new}RH + f_{new}$$

$$\tag{14}$$

where a_{new}, b_{new}, c_{new}, d_{new}, e_{new}, and f_{new} are empirical coefficients. In this study, these coefficients were determined as 1.06, 42.18, 4.90, -1.97, 0.89, and -178.28 respectively. Figure 3(a) shows that the overall training accuracy of the estimated all-sky ocean-surface R_l from Modnew was satisfactory, yielding an R^2 of 0.89, RMSE of 9.87 W/m^2, and nearly no bias. Afterwards, Equation (14) was used to determine the hourly ocean-surface R_l based on the corresponding hourly training samples (see Table 4). The hourly results shown in Figure 3(b) were satisfactory, with an R^2 of 0.78, RMSE of 15.44 W/m^2, and nearly no bias. Note that the R_l measurements whose values were larger than 450 W/m^2 were thought to be unreasonable and were manually removed (see Section 3.1).

492
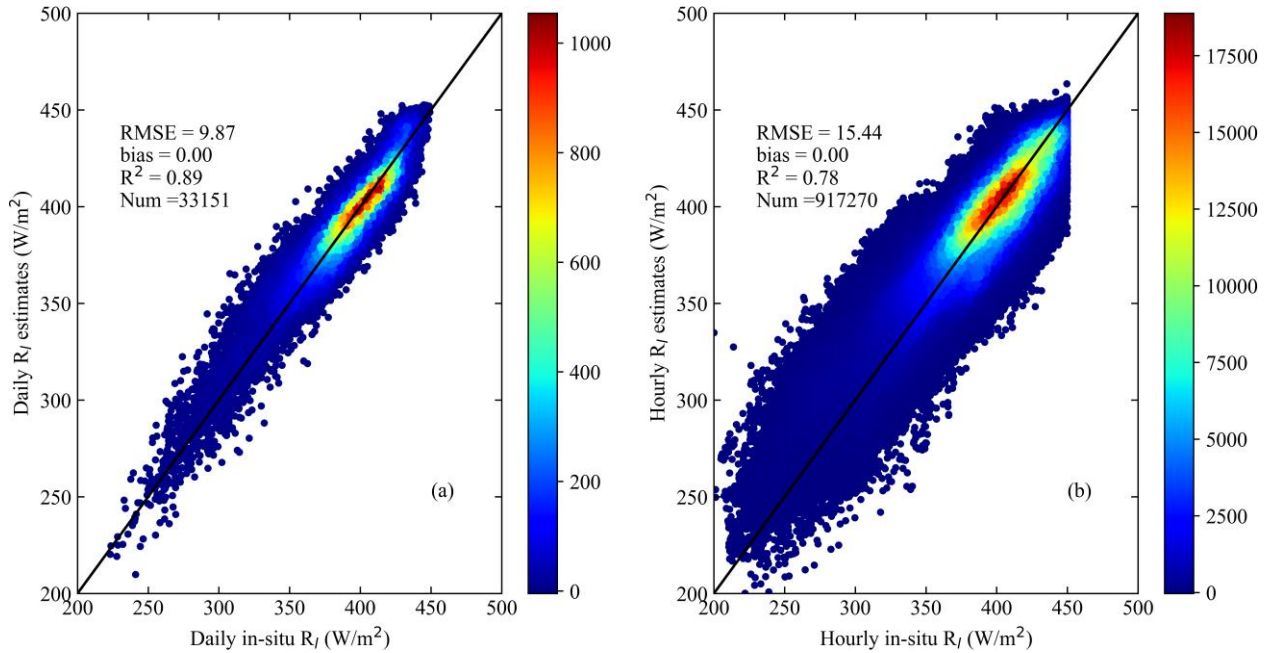
Figure 3. Overall training accuracy of the all-sky daily R_l at (a) daily and (b) hourly scales. In
panels a and b, the color bar represents points per unit area.

495

496   By considering the influence of the calculated cloud cover on the R_l estimates, the hourly
497 results were separated into daytime and nighttime, respectively, as shown in Figure 4. The
498 training accuracy of the daytime sample was higher than that at nighttime, with R^2 values of 0.82
499 and 0.79 and RMSE values of 13.18 and 16.24 W/m^2, respectively. It was assumed that the larger
500 uncertainties in the hourly ocean-surface R_l at nighttime were possibly owing to the estimated
501 cloud cover, which might have an influence on Modnew in the form of overestimating R_l.
502 Overall, the performance of Modnew was very good, both at daily and hourly scales for all-sky
503 R_l estimation at the ocean surface.
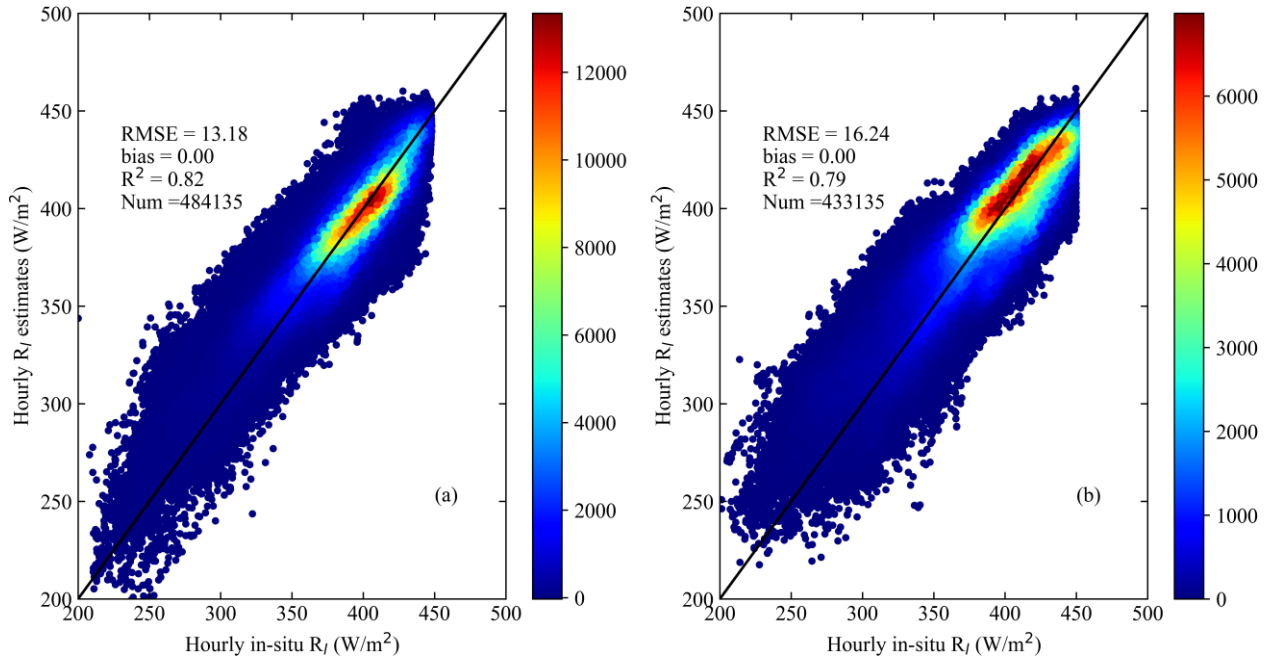
Figure 4. Overall training accuracy of the all-sky hourly R_l during (a) daytime and (b) nighttime. The color bars represent points per unit area.

4.2 Model comparison results

Based on the independent validation samples, Mod1–Mod8 and Modnew were validated one by one and compared for various cases (Table 4). Before that, the eight existing models were calibrated using the corresponding training samples, which means that Mod1–Mod5 were calibrated with the clear-sky training hourly/daily samples, while Mod6–Mod8 were calibrated with the all-sky training hourly/daily samples, i.e., the same as Modnew. Afterwards, these models were validated against the matched validation samples for each case. The updated coefficients of Mod1–Mod8 and the coefficients of Modnew for hourly and daily scales are given in Table 5. For better illustration, the comparison results are presented for clear- and all-sky conditions in the following paragraphs.

Table 5

Coefficients of the Nine Models Used for Hourly/Daily Ocean-surface R_l Estimation. The Values in Parentheses are the Uncertainties of the Fitted Parameters

Models	a	b	c	d	e	f
Hourly						
Mod1	$0.675(\pm 6 \times 10^{-4})$	$0.052(\pm 3 \times 10^{-4})$	/	/	/	/
Mod2	$0.246(\pm 1 \times 10^{-4})$	$7.77 \times 10^{-4}(\pm 0.03)$	/	/	/	/
Mod3	$1.21(\pm 9 \times 10^{-5})$	/	/	/	/	/
Mod4	$1.056(\pm 8 \times 10^{-5})$	/	/	/	/	/
Mod5	$7.48(\pm 0.01)$	$1.28(\pm 0.003)$	$0.5(\pm 0.005)$	/	/	/
Mod6	$0.229(\pm 4 \times 10^{-4})$	$-0.006(\pm 8 \times 10^{-5})$	/	/	/	/
Mod7	$0.812(\pm 2 \times 10^{-4})$	$0.001(\pm 7 \times 10^{-6})$	$0.121(\pm 1 \times 10^{-4})$	/	/	/
Mod8	$-5.557(\pm 0.38)$	$13.378(\pm 0.35)$	$82.43(\pm 1.21)$	$0.85(\pm 0.02)$	$85.33(\pm 0.60)$	/

Modnew	0.986(±6 ×10⁻⁴)	40.991(±0.05)	3.116(±0.01)	-2.478(±0.01)	0.921(±0.02)	-144.62(±0.30)

Models						
Daily						
Mod1	0.65(±0.004)	0.06(±0.001)	/	/	/	/
Mod2	0.25(±0.003)	7.77×10⁻⁴(±0.18)	/	/	/	/
Mod3	1.21(±5 ×10⁻⁴)		/	/	/	/
Mod4	1.061(±5 ×10⁻⁴)	/	/	/	/	/
Mod5	1.69(±0.09)	2.67(±0.25)	0.5(±0.02)	/	/	/
Mod6	0.286(±0.002)	-0.03(±3 ×10⁻⁴)	/	/	/	/
Mod7	0.805(±0.002)	0.002(±8 ×10⁻⁵)	0.133(±0.01)	/	/	/
Mod8	-0.34(±0.02)	8.545(±0.19)	-12.19(±0.59)	0.08(±0.009)	0.08(±0.006)	/
Modnew	1.06(±0.002)	42.18(±0.22)	4.90(±0.06)	-1.97(±0.04)	0.89(±0.008)	-178.28(±1.15)

4.2.1 Clear sky

All models, including the eight previous models (Mod1–Mod8), and the newly developed model (Modnew), could be used under clear-sky conditions at both hourly and daily scales with the updated coefficients given in Table 5.

4.2.1.1 Hourly scale

Table 6 shows the validation results of the nine models under clear-sky conditions at the hourly scale. Meanwhile, the validation results of Mod1–Mod8 with their original coefficients (see Section 2) are also presented in Table 6, using the same validation samples for comparison.

Table 6
Overall Validation Accuracy of the Nine Ocean-surface R_l Models under Clear-sky Conditions at the Hourly Scale. The Values in Parentheses for Mod1–Mod8 are the Validation Results Found Using Their Original Coefficients

Models	R^2	RMSE(W/m^2)	bias(W/m^2)
Mod1	0.77 (0.78)	14.69 (15.43)	-0.42 (-0.88)
Mod2	0.71 (0.71)	16.37 (16.61)	-0.31 (-2.80)
Mod3	0.77 (0.77)	14.77 (17.87)	-0.53 (9.84)
Mod4	0.74 (0.74)	15.53 (17.11)	-0.22 (7.33)
Mod5	0.77 (0.77)	14.62 (26.90)	-0.44 (-19.56)
Mod6	0.75 (0.77)	16.87 (21.51)	7.33 (15.28)
Mod7	0.74 (0.77)	18.37 (17.52)	9.27 (-9.57)
Mod8	0.78 (0.78)	15.59 (37.00)	2.45 (-33.27)
Modnew	0.79	14.82	4.40

The validation results illustrate that most models estimated the clear-sky hourly ocean-surface R_l with a similar accuracy, with R^2 values ranging from 0.74 to 0.79, RMSE values ranging from 14.62 to 18.37 W/m^2, and bias values ranging from -0.53 to 9.27 W/m^2 (Table 6). All eight existing models with the calibrated coefficients had a higher accuracy than those with the original coefficients except Mod7; in particular, the RMSE of Mod8 decreased by ~21 W/m^2. The magnitude of the bias of Mod1–Mod8 also decreased after recalibration, with the magnitudes of the biases of Mod1–Mod5 being much smaller than those of Mod6–Mod8 and Modnew, which were trained with the all-sky hourly samples. Among the four all-sky models, the newly developed Modnew performed the best, with the largest R^2 of 0.79, the smallest RMSE of 14.82 W/m^2.

542 Then, the hourly validation results of the nine models were further examined using the
543 daytime and nighttime values separately, which are shown in Figure 5. The performance of most
544 models, including the five clear-sky models (Mod1–Mod5) and one all-sky model (Mod8), in
545 estimating the hourly clear-sky R_l during the daytime was much better than that at nighttime,
546 with RMSE values at daytime and nighttime ranging from ~12.50 to 15.06 W/m² and 16.80 to
547 19.50 W/m², respectively. ~~On the contrary~~In contrast, the performances of Mod6–Mod7 and
548 Modnew were better at nighttime than that at daytime, with RMSE values at daytime and
549 nighttime ranging from ~15.00 to 19.20 W/m² and 14.40 to 16.60 W/m², respectively. Regarding
550 the bias values, at nighttime, all five clear-sky models had a significant underestimation problem
551 (negative biases), while the all-sky models had smaller bias values. This may be due to the
552 uncertainty in the calculated CI at nighttime, which could influence the cloud determination and
553 then R_l. In addition, among the five clear-sky models, Mod2 based only on air temperature shows
554 the lowest accuracy in terms of RMSE during both daytime and nighttime. Among the nine
555 models, Modnew had the most stable performance in hourly R_l estimation under clear-sky
556 conditions during both daytime and nighttime with similar RMSE values of 15.03 and 14.38
557 W/m², respectively, where in particular its nighttime R_l estimation accuracy was the best among
558 the nine models.

559
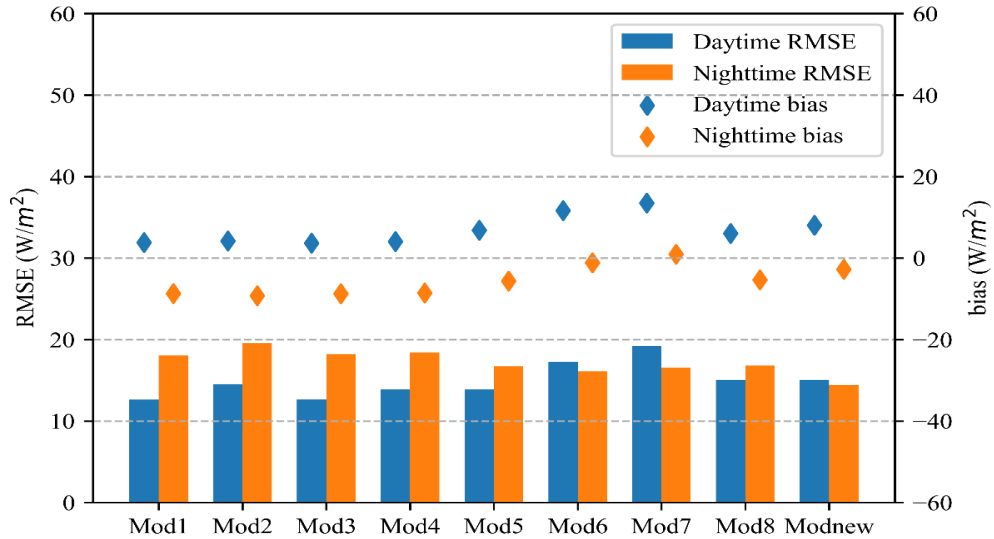
560 **Figure 5.** Validation accuracy of the estimated R_l under clear-sky conditions at the hourly scale
561 for the nine models represented by RMSE (left axis) and bias (right axis).

562 Furthermore, the four all-sky R_l estimation models (Mod6–Mod8 and Modnew) were also
563 trained using the clear-sky hourly samples, and their outputs were validated against the in situ
564 observations. The estimation accuracy of the four all-sky models all improved after calibration:
565 their overall validated RMSE values decreased to ~13.40 to 15.40 W/m² and ~12.01 to 14.29
566 W/m² during the daytime, slight decreases (~1 W/m²) at nighttime, and their biases values tended
567 to 0. This indicates that the ability of the four all-sky models in estimating clear-sky hourly R_l
568 was comparable with or even better than the other five models which only work for clear-sky
569 conditions. Indeed, Modnew performed the best of all models during either daytime or nighttime,
570 with corresponding validated RMSE values of 12.01 and 16.00 W/m², respectively.

 4.2.1.2 Daily scale

As for the results at the daily scale, the nine evaluated models were trained with the corresponding daily training samples (see Table 4) and validated against the in situ measurements. As shown in Table 7, the estimation accuracy of the daily clear-sky ocean-surface R_l from nearly all previous models improved significantly after recalibration, where the RMSE values and the magnitudes of the bias decreased by up to ~4 W/m^2 and ~9 W/m^2, respectively, except for Mod7. The five clear-sky models (Mod1–Mod5) performed much better than the three previous all-sky models (Mod6–Mod8), with RMSE values ranging from 9.58 to 11.43 W/m^2 and 14.02 to 15.69 W/m^2, and biases values ranging from 0.11 to 0.57 W/m^2 and 4.99 to 9.53 W/m^2, respectively. Besides, the Mod2 still exhibited lower accuracy than the other four clear-sky models, with the highest validated RMSE value of 11.43 W/m^2. The performance of Modnew was the best among the four all-sky models, with the smallest validated RMSE value of 10.76 W/m^2 and bias of 3.53 W/m^2. Similar to the hourly results under the clear-sky conditions, the validation results improved considerably if all four all-sky models were trained using the clear-sky daily samples: their RMSE values and biases decreased to ~8−13 W/m^2 and were nearly zero, respectively, which were even better than the corresponding decreases measured for Mod1 to Mod5. Modnew was the best in comparison to the other three all-sky models, in this case yielding an RMSE of 8.36 W/m^2.

Table 7
Overall Validation Accuracy of the Nine Ocean-surface R_l Models under Clear-sky Conditions at the Daily Scale. The Values in Parentheses for Mod1–Mod8 are the Validation Results Found Using Their Original Coefficients

Models	R^2	RMSE(W/m^2)	bias(W/m^2)
Mod1	0.89 (0.90)	9.66 (11.16)	0.38 (-2.00)
Mod2	0.85(0.85)	11.43 (11.91)	0.45 (-3.35)
Mod3	0.90(0.90)	9.87 (13.57)	0.11 (9.06)
Mod4	0.88(0.88)	10.50 (12.62)	0.57 (7.16)
Mod5	0.89 (0.89)	9.58 (11.92)	0.39 (6.97)
Mod6	0.87 (0.88)	14.32 (18.43)	9.53 (15.26)
Mod7	0.87 (0.88)	14.02 (13.67)	8.15 (-9.18)
Mod8	0.80 (0.81)	15.69 (19.63)	4.99 (-12.56)
Modnew	0.89	10.76	3.53

In summary, for the ocean-surface R_l estimation under clear-sky conditions, the use of an all-sky model trained with the clear-sky samples is recommended at both hourly and daily scales. Modnew performed the best of all nine models when trained with the clear-sky samples, and was comparable with the other five clear-sky models when trained with the all-sky samples. Furthermore, our validation results show that the accuracy of Mod2 is not as high as that of other clear-sky models that include water vapor variable in terms of RMSE.

4.2.2 All sky

4.2.2.1Hourly scale

Table 8 gives the overall validation results of the all-sky hourly scale ocean-surface R_l from the four models against the independent validation samples with the updated and original coefficients, respectively.

Table 8

 Overall Validation Accuracy of Four Ocean-surface R_l Models under All-sky Conditions at the
606 *Hourly Scale. The Values in Parentheses for Mod6–Mod8 are the Validation Results Found*
607 *Using Their Original Coefficients*

Models	R^2	RMSE(W/m^2)	bias(W/m^2)
Mod6	0.67 (0.65)	18.53 (19.84)	0.05 (3.83)
Mod7	0.66 (0.64)	19.06 (26.10)	-0.14 (-10.27)
Mod8	0.74 (0.51)	16.91 (37.33)	-0.41 (-28.47)
Modnew	0.76	15.95	-0.04

608   Compared to the results in Table 6, the estimation accuracies under all-sky conditions
609 shown in Table 8 were generally worse, with lower R^2 values (0.66–0.76) and bigger RMSE
610 values (15.95–19.06 W/m^2), which indicates that the uncertainty in the cloud information was the
611 major reason for the increased uncertainty in the R_l estimation. As in previous results, the three
612 previous models, Mod6–Mod8, performed much better after recalibration, with decreased RMSE
613 values up to ~20 W/m^2 and their bias values tended to 0; Mod7 still performed the worse.
614 Modnew performed the best, with an RMSE of 15.95 W/m^2 and a bias of -0.04W/m^2, followed
615 by Mod8.
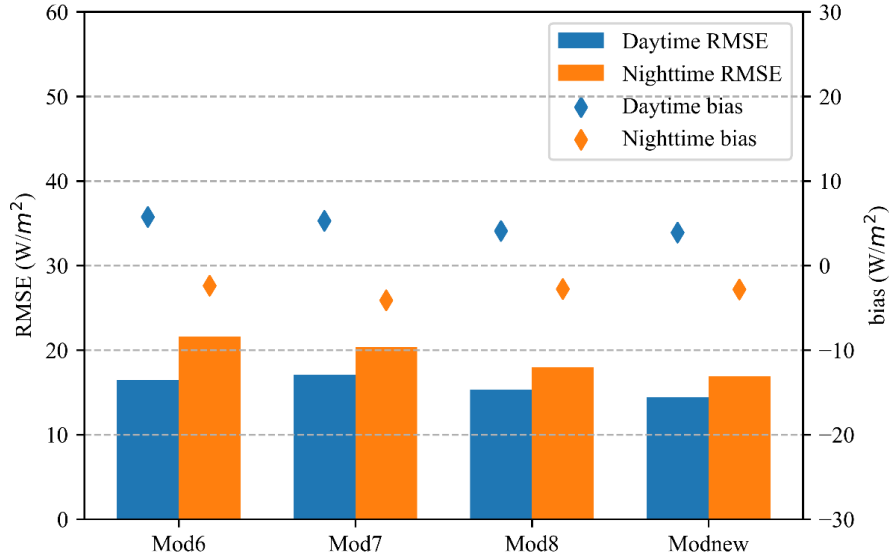
616
Figure 6. Validation accuracy of the estimated Rl under all-sky conditions at the hourly scale for
618 Mod6-Mod8 and Modnew represented by RMSE (left axis) and bias (right axis).

619   The hourly results in Table 8 were examined for daytime and nighttime values, as shown
620 in Figure 6. The results show that the estimation accuracies of the four models were overall
621 better during the daytime than at nighttime, with smaller RMSE values for the former.
622 Specifically, during daytime hours, the accuracy of Modnew was similar to that of Mod8, with
623 RMSEs of 14.43 and 15.33 W/m^2, respectively, which were better than those of Mod6 and
624 Mod7, which yielded RMSEs of 16.46 and 17.09 W/m^2, respectively. However, Mod7 performed
625 a little bit better than Mod6 during the nighttime, although its overall performance was the worst.
626 It is speculated that the larger uncertainties in the all-sky ocean-surface R_l values at nighttime
627 can possibly be attributed to the cloud information at nighttime, which was difficult to estimate
628 accurately compared to the daytime cloud information.

629   4.2.2.2 Daily scale

630   Figure 7 shows the overall validation accuracies of the all-sky daily ocean-surface R_l
631   values from the four models. Compared with Mod6–Mod8, Modnew had the best performance,
632   with an validated RMSE of 10.27 W/m^2, a bias of 0.10 W/m^2, and an R^2 of 0.88, followed by
633   Mod8, which yielded an RMSE of 11.96 W/m^2, a bias of -0.18 W/m^2, and an R^2 of 0.85.
634   However, Mod8 had a tendency to overestimate low values (<300 W/m^2), as did Mod6 and
635   Mod7.

636
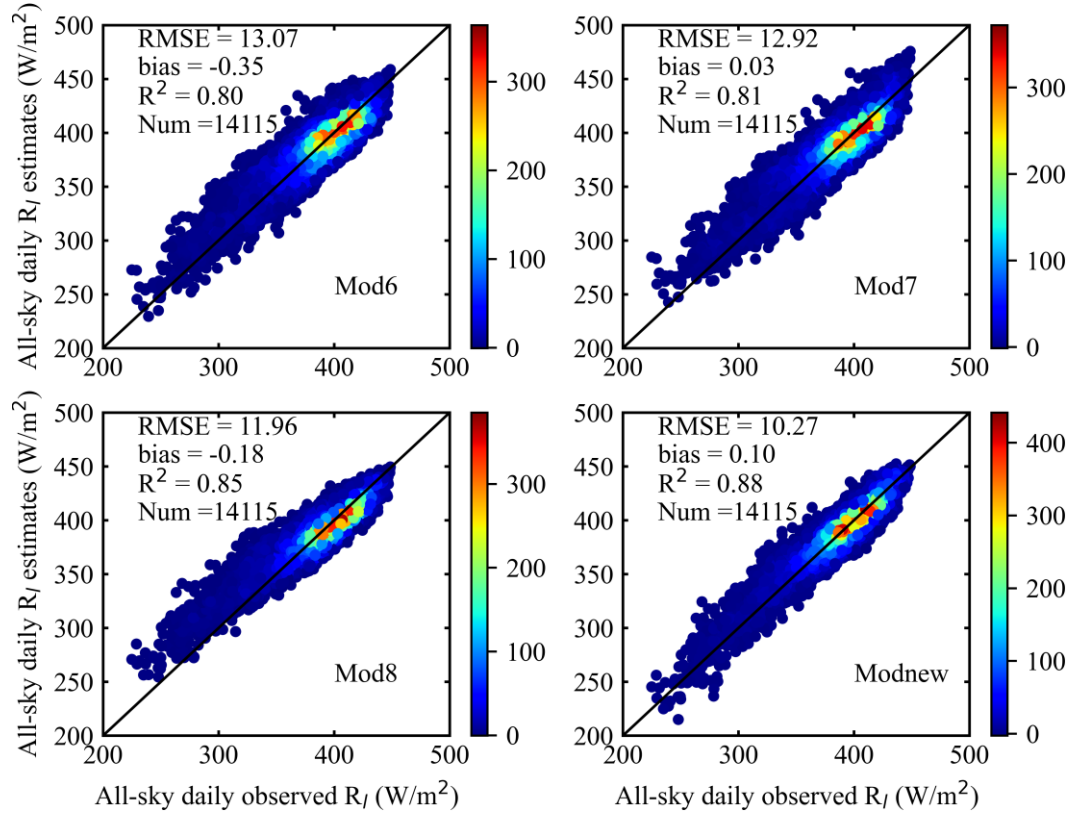
637   **Figure 7.** Overall validation result of the calculated all-sky daily ocean-surface R_l from the four

638   models against the independent moored measurements. The color bars represent points per unit

639   area.

640   Overall, it is speculated that Modnew performed better than Mod6–Mod8 because of the
641   introduction of two cloud-related parameters (clw and ciw) into the model in addition to the
642   cloud fraction. In order to demonstrate this speculation better, the relationship between the
643   estimation errors in the daily all-sky ocean-surface R_l of the four models and clw, which was
644   used to represent the CBH, was further analyzed. The corresponding mean of the estimation
645   errors in the daily all-sky ocean-surface R_l and its SEM for each bin of clw in logarithmic format
646   (in 10% increments) were calculated, as presented in Figure 8.
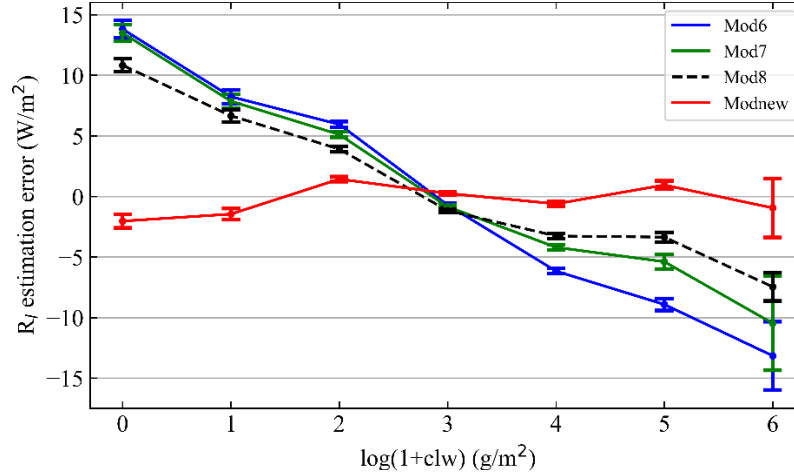
Figure 8. The averaged R_l estimation errors and its SEM of Mod6 – Mod8 and Modnew varied with clw in logarithmic format.

From the results in Figure 8 it can be seen that the R_l estimation errors of Mod6–Mod8 were negative linearly related to increasing log(1+clw); such behavior is not seen for Modnew. This indicates that the cloud information related to the variations in daily ocean-surface R_l are not fully characterized by only the cloud fraction. Although Mod8 performed better than Mod6 and Mod7 because of the introduction of the dew point depression to compensate for the difference between the surface temperature and cloud base temperature, the contributions of the cloud base emission to R_l still cannot be thoroughly expressed over the ocean surface. Hence, Modnew performed superior to other models because it also takes clw as input. Moreover, ciw was also introduced in Modnew to ensure its robust performance at high latitudes.

4.3 Further analysis on Modnew

Based on the direct validation results described above, Modnew satisfactorily estimated the ocean-surface R_l under both clear- and all-sky conditions at both hourly and daily scales. Hence, further analysis of this new model, such as testing its performance robustness and a sensitivity analysis, was conducted, and the results are given below.

4.3.1 Modnew performance analysis

In order to examine the robustness of its performance, the spatial distributions of the validation accuracies of the all-sky R_l estimates from Modnew at the moored buoy sites are presented in Figures 9(a–b) for hourly and daily scales, respectively. Note that the moored buoy data from which the number of provided validation samples were less than 50 were excluded to provide a more objective comparison.
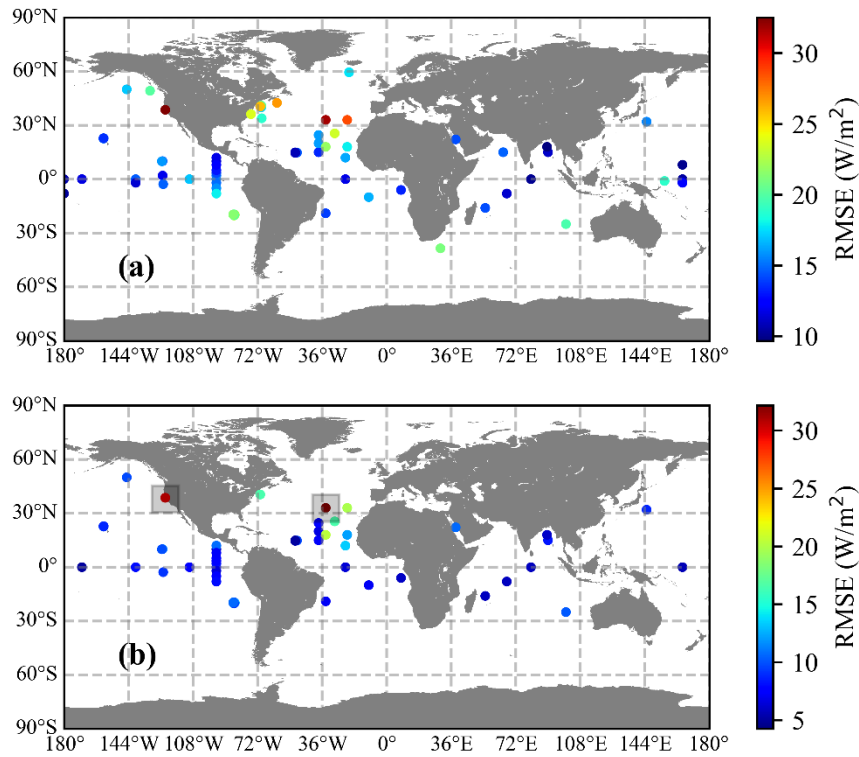
Figure 9. Validation accuracies of Modnew on the hourly scale (a) and daily scale (b) at different sites represented by the RMSE values. The two moored buoys in the shaded boxes in (b) are UOP_SMILE88 (38°N, 123.5°W) and UOP_SUB_NW (33°N, 34°W).

The spatial distribution of the validation accuracy (represented by RMSE) of the R_l estimates from Modnew was similar for the hourly and daily data. Their RMSE values got larger from tropical to the high latitude seas, although the daily R_l estimates were generally more accurate than the hourly ones, and the validation accuracy for sites at open seas was more accurate than that within coastal seas. For a better illustration, two time series of the estimated daily ocean-surface R_l from Modnew at two sites were randomly selected and shown in Figure 10, and the one from Mod8 was added for comparison, as well as the corresponding scatter plots. The two buoys, TAO_03 (0°N, 140°W) and OS_PAPA (50°N, 145°W), are in equatorial and mid-high latitude seas, respectively. The temporal variations in the all-sky daily R_l estimates from the two models both captured the variations in the moored R_l measurements very well, but the ones from Modnew were closer to the measurements at high values and low values, especially at the OS_PAPA site. The validation accuracy of Modnew was higher than that of Mod8 at both sites, and Modnew performed better for tropical seas, with validated RMSE values of 6.73 and 10.00 W/m^2, respectively, which was assumed that more samples used for modeling were collected at tropical seas and this would influence the model performance at mid-high latitude seas.
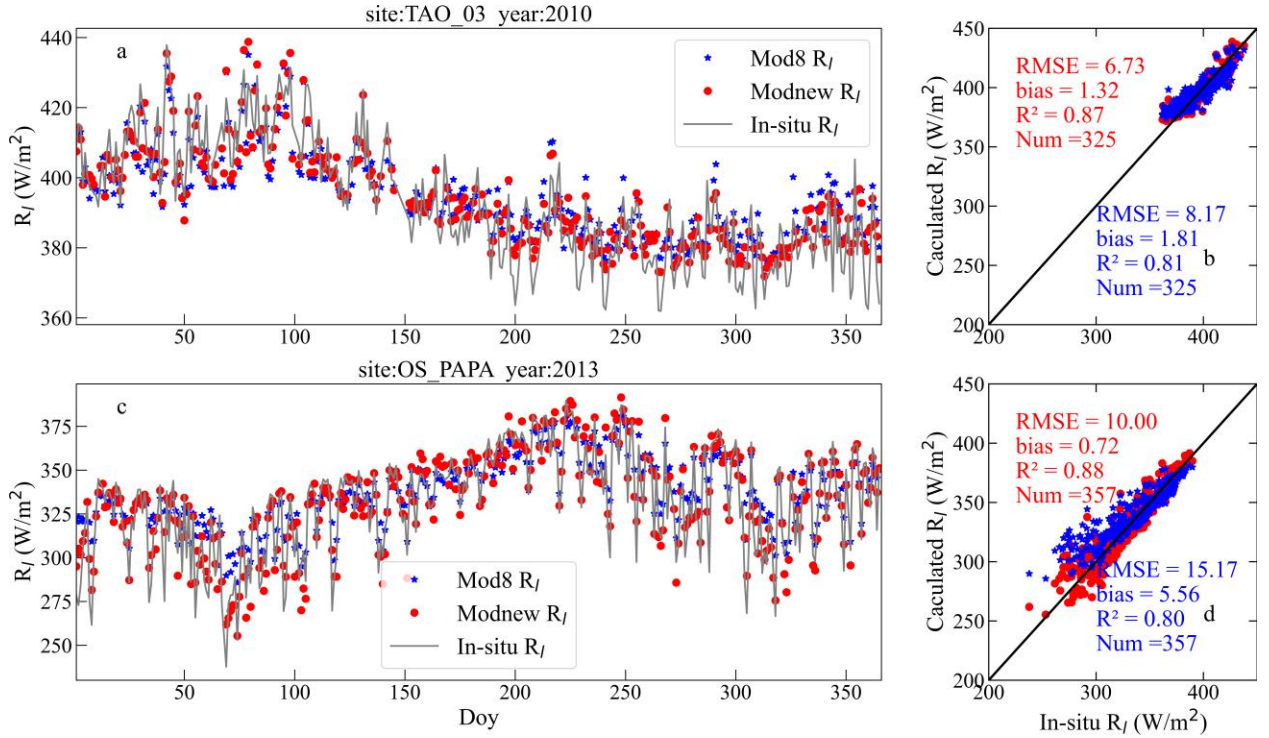
Figure 10. Time series and scatter plots of the R_l estimates and the moored R_l measurements at the (a–b) TAO_03 (0°N, 140°W) and (c–d) OS_PAPA (50°N, 145°W) sites. The red points and blue points represent Modnew and Mod8, respectively.

However, it was noted that Modnew performed poor at some sites, such as UOP_SMILE88 (38°N, 123.5°W) and UOP_SUB_NW (33°N, 34°W) (see the shaded boxes in Figure 9). The estimation errors in the daily R_l from Modnew at the two moored buoys were calculated, as shown in Figure 11, and the ones from the other three all-sky models, Mod6–Mod8, are shown for comparison. It can be seen that the four evaluated all-sky models all worked poorly at the two sites, all giving overestimations. A possible explanation may be attributed to the differences in the characteristics of the atmospheric boundary layer over the two sites relative to the open sea. Specifically, UOP_SMILE88 is deployed on the northern California shelf, which is influenced by air temperature inversions (ATIs) (Dorman et al., 1995), and UOP_SUB_NW is deployed near the eastern flank of the Azores anticyclone system (Moyer & Weller, 1997). As such, the atmospheric conditions of the two sites are different from those over the open sea, which would affect the estimation of R_l made with models whose coefficients were determined by samples collected mostly from sites located in the open sea. Therefore, more samples should be collected within these seas to help to improve the ocean-surface R_l estimation accuracy in these areas.
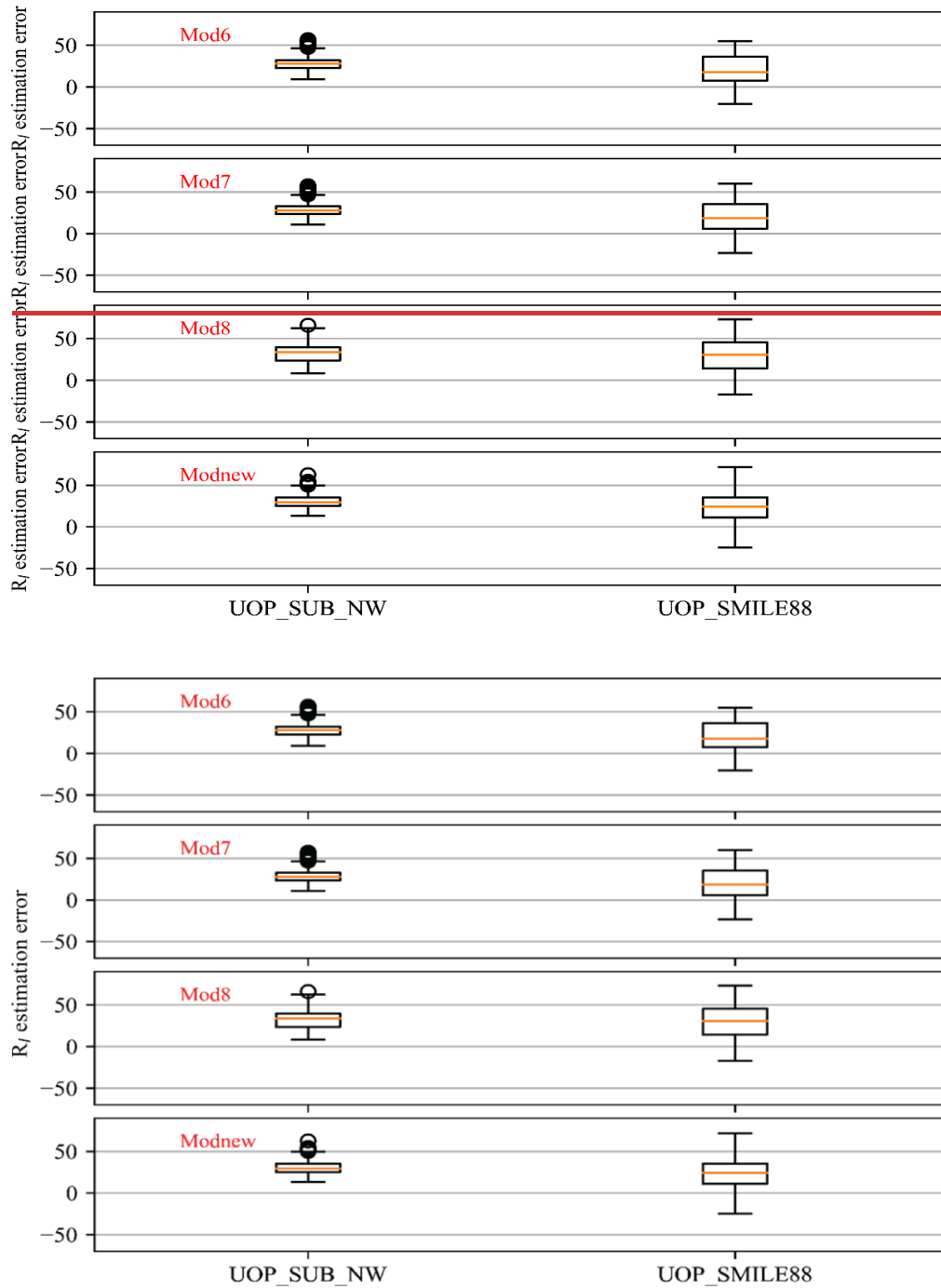
Figure 11. Box plots of the R_l estimation errors from models Mod6, Mod7, Mod8, and Modnew at UOP_SMILE88 (38°N, 123.5°W) and UOP_SUB_NW (33°N, 34°W). The top edge, center, and bottom edge of the box represent the 75th, 50th (median), and 25th percentiles, respectively. The whiskers indicate the maximum and minimum values within 1.5 times the interquartile range (IQR), and the circles denote outliers.

4.3.2 Sensitivity analysis

In order to quantify the impact of each parameter on the calculated R_l in Modnew, the SimLab software (http://simlab.jrc.ec.europa.eu) was used to conduct a global sensitivity analysis. All inputs in Modnew (T_a, RH, C, clw, and ciw) were entered into the software separately, and then 2,000 ocean-surface R_l values were calculated using Modnew by taking 2,000 combinations of these parameters as inputs. Afterwards, the Fourier amplitude sensitivity test (FAST) method (Saltelli et al., 1999) in the SimLab software was employed to conduct a sensitivity analysis based on the inputs, and the corresponding estimated R_l values were used for a sensitivity analysis using the total sensitivity index (TSI). The TSI indicates each parameter's total contribution to the output variance when the interactions of other parameters are also considered, and was used to quantify the sensitivity of each parameter. Table 9 shows the TSI of each parameter in Modnew. Specifically, T_a had the most important effect on R_l with the largest TSI of 41.26%, followed by C (25.6%) and RH (21%). Therefore, the performance of Modnew mainly depended on the accuracy of the T_a, C, and RH. The TSI of clw was the fourth highest with 8%, but it is essential to supplement cloud information that cloud cover alone cannot provide, especially for cloud-sky conditions. In terms of ciw, its TSI was just 0.008, which was possibly because only a few samples at high-latitudes were used in this study.

Table 9

FAST Sensitivity Indices of the First Order for Each Input Variable in Modnew

T_a	RH	C	Clw	ciw
0.4126	0.21	0.256	0.08	0.008

5 Conclusions

Due to the significance of R_l at the ocean surface, many empirical models have been established for ocean-surface R_l calculation based on observations by relating R_l to some climatic factors, such as T_a, RH, and so on. However, most models were developed only for clear days, and for those models that can calculate the all-sky R_l, only the cloud cover is taken into account, which is thought to be insufficient for characterizing the influence of clouds on R_l, especially for ocean surfaces where cloudy skies are common. Indeed, most previous R_l estimation models were developed only within a specific region based on limited observations, and some for just land surfaces. Consequently, there was a need to perform comprehensive evaluations of these models, including their ability to predict R_l over global seas.

In this study, ~~a new model called Modnew, in which the all-sky ocean-surface R_l is nonlinearly related to T_a, RH, C, clw, and ciw, has been successfully developed.~~ the newly developed Modnew model estimates all-sky ocean-surface downward longwave radiation (R_l) by incorporating key atmospheric and cloud parameters: screen-level air temperature (Ta), relative humidity (RH), fractional cloud cover (C), total column cloud liquid water (clw), and total column cloud ice water (ciw). Ta governs the thermal radiation emitted by the atmosphere, as described by the Stefan–Boltzmann law. RH modifies the atmospheric emissivity by representing the water vapor content. C quantifies the cloud's overall presence, while clw and ciw capture the thermal contributions of liquid and ice clouds, respectively, enabling a more accurate characterization of cloud radiative effects. The Modnew model relies on specific atmospheric and cloud-related parameters for accurate R_l estimation. While inputs such as Ta and RH are

commonly obtained from in situ measurements, critical cloud-related parameters (i.e. clw and ciw) are typically derived from satellite products or reanalysis datasets, such as ERA5. These parameters are essential for capturing the radiative properties of clouds, which in situ measurements alone cannot reliably provide. Therefore, satellite data or reanalysis products are indispensable for supplying these inputs. This model, as well as eight comparison models, was used to estimate the all-sky ocean-surface R_l at both hourly and daily scales based on comprehensive observations collected from 65 globally distributed moored buoys from 1988 to 2019. In contrast to previous models, Modnew incorporates more cloud-related parameters (i.e., clw and ciw) into the model besides just cloud cover. Modnew and the eight previous R_l models were assessed against the moored values for various cases, including clear- and all-sky conditions at daytime and nighttime and at hourly and daily scales. After careful analysis, several major conclusions could be drawn, as follows:

(1) The eight previous models performed much better after calibration of their coefficients with the global observations for almost all cases, except Mod7 in some situations.

(2) For the clear-sky ocean-surface R_l estimation, the four all-sky models (Mod6–Mod8 and Modnew) could work comparably to or even better than the five clear-sky models (Mod1–Mod5) if their coefficients were calibrated by the clear-sky samples, yielding overall validated RMSE values ranging from 13.40 to 15.40 W/m^2 at the hourly scale and 8.00–13.00 W/m^2 at the daily scale. In terms of daytime and nighttime, all five clear-sky models (Mod1–Mod5) performed better at daytime than that at nighttime, and vice versa for the four all-sky models except Mod7. Mod1–Mod5 generally had the tendency to underestimate R_l at nighttime because they do not consider the influence of clouds. Among all models, Modnew was the most robust, yielding RMSE values of 15.03 W/m^2 and 14.38 W/m^2 at daytime and nighttime for the hourly scale, respectively.

(3) For the all-sky ocean-surface R_l estimation, the performance of the four evaluated models was generally worse compared to that under clear-sky conditions, which further demonstrated that the uncertainty in the all-sky R_l estimation was highly dependent on accurate cloud information. Specifically, at the hourly scale, the validated RMSE values of the four models ranged from 15.95 to 19.06 W/m^2, with better performance at daytime. At the daily scale, the RMSE values ranged from 10.27 to 13.07 W/m^2. Modnew also performed the best in these cases, with an overall validated RMSE of 15.95 and 10.27 W/m^2 and bias values of -0.04 and 0.10 W/m^2, respectively. It is worth noting that Modnew performed similarly during both daytime and nighttime at the hourly scale.

In summary, the performance of Modnew was superior to other previous models for ocean-surface R_l estimation for any case, which was mainly because of the introduction of more cloud-related information (clw and ciw). Further analysis of Modnew illustrated the significance of the two parameters as well as cloud cover. However, all results again emphasized that the accuracy of nearly all the empirical models was highly dependent on the spatial distribution, quality, and quantity of the samples used for modeling. For instance, Modnew worked better at open seas in tropical regions where more samples were available compared to other regions. Therefore, many more samples at different regions, such as in coastal regions and high-latitude seas, should be collected in the future to improve model performance. Moreover, more accurate cloud information especially at nighttime is essential to decrease the uncertainty in the estimated R_l at the ocean surface.

Competing interests

The contact author has declared that none of the authors has any competing interests.

Acknowledgments

We acknowledge the buoy data sets provided by UOP, GTMBA, and OceanSITES project. We are grateful to ECMWF for providing the reanalysis data sets. We would also like to thank the contributions made by the anonymous reviewers and editor that helped improve the quality of this paper.

Funding

This work was supported by the Natural Science Foundation of China (41971291).

Data availability

All data sets used in this research, including the moored buoy observations and satellite and reanalysis data are publicly available. Detailed information on these data sets, including citations and web links, is presented in Section 3.

Author contributions.

PJH and BJ designed and performed the study. All authors contributed to the analysis of results and final version of the paper.

References

Aase, J. K., & S. B. Idso (1978), A comparison of two formula types for calculating long-wave radiation from the atmosphere, Water Resour Res, 14(4), 623-625, https://doi.org/10.1029/WR014i004p00623.
Alados, I., I. Foyo-Moreno, & L. Alados-Arboledas (2012), Estimation of downwelling longwave irradiance under all-sky conditions, Int J Climatol, 32(5), 781-793, https://doi.org/10.1002/joc.2307.
Alappattu, D. P., Q. Wang, R. Yamaguchi, R. J. Lind, M. Reynolds, & A. J. Christman (2017), Warm layer and cool skin corrections for bulk water temperature measurements for air-sea interaction studies, J Geophys Res-Oceans, 122(8), 6470-6481, https://doi.org/10.1002/2017jc012688.
Bignami, F., S. Marullo, R. Santoleri, & M. E. Schiano (1995), Longwave radiation budget in the Mediterranean Sea, J Geophys Res-Oceans, 100(C2), 2501-2514, https://doi.org/10.1029/94jc02496.
Bilbao, J., & A. H. de Miguel (2007), Estimation of Daylight Downward Longwave Atmospheric Irradiance under Clear-Sky and All-Sky Conditions, J. Appl. Meteor. Climatol., 46(6), 878-889, https://doi.org/10.1175/jam2503.1.
Bourlès, B., R. Lumpkin, M. J. McPhaden, F. Hernandez, P. Nobre, E. Campos, et al. (2008), The PIRATA program: History, accomplishments, and future directions, Bull. Amer. Meteor. Soc., 89(8), 1111-1126, https://doi.org/10.1175/2008bams2462.1.
Brunt, D. (1932), Notes on radiation in the atmosphere, Quart J Roy Meteor Soc, 58, 389-420.
Brutsaert, W. (1975), On a derivable formula for longwave radiation from clear skies, Water Resour Res, 11(5), 742-744, https://doi.org/10.1029/WR011i005p00742.
Buck, A. L. (1981), New equations for computing vapor pressure and enhancement factor, J Appl Meteorol, 20(12), 1527-1532, https://doi.org/10.1175/1520-0450(1981)020<1527:NEFCVP>2.0.CO;2.

837   Caniaux, G. (2005), A 1 year sea surface heat budget in the northeastern Atlantic basin during the POMME
838   experiment: 1. Flux estimates, J. Geophys. Res., 110(C7), https://doi.org/10.1029/2004jc002596.
839   Centurioni, L. R., J. Turton, R. Lumpkin, L. Braasch, G. Brassington, Y. Chao, et al. (2019), Global in situ
840   observations of essential climate and ocean variables at the air–sea interface, Front Mar Sci, 6, 419,
841   https://doi.org/10.3389/fmars.2019.00419.
842   Clark, N. E., L. Eber, R. M. Laurs, J. A. Renner, & J. F. T. Saur (1974), Heat exchange between ocean and
843   atmosphere in the eastern North Pacific for 1961–71, Tech. Rep. NMFS SSRF-682, NOAA, U.S. Dept. of Commer.,
844   Washington, D. C.
845   Cleugh, H. A., R. Leuning, Q. Mu, & S. W. Running (2007), Regional evaporation estimates from flux tower and
846   MODIS satellite data, Remote Sens Environ, 106(3), 285-304, https://doi.org/10.1016/j.rse.2006.07.007.
847   Cottier, F. R., F. Nilsen, M. E. Inall, S. Gerland, V. Tverberg, & H. Svendsen (2007), Wintertime warming of an
848   Arctic shelf in response to large-scale atmospheric circulation, Geophys Res Lett, 34(10),
849   https://doi.org/10.1029/2007GL029948.
850   Cronin, M. F., C. L. Gentemann, J. Edson, I. Ueki, M. Bourassa, S. Brown, et al. (2019), Air-sea fluxes with a focus
851   on heat and momentum, Front Mar Sci, 6, https://doi.org/10.3389/fmars.2019.00430.
852   Deremble, B., N. Wienders, & W. K. Dewar (2013), CheapAML: A simple, atmospheric boundary layer model for
853   use in ocean-only model calculations, Mon. Wea. Rev., 141(2), 809-821, https://doi.org/10.1175/MWR-D-11-
854   00254.1.
855   Diak, G. R., W. L. Bland, J. R. Mecikalski, & M. C. Anderson (2000), Satellite-based estimates of longwave
856   radiation for agricultural applications, Agr Forest Meteor., 103(4), 349-355, https://doi.org/10.1016/S0168-
857   1923(00)00141-6.
858   Doelling, D. R., N. G. Loeb, D. F. Keyes, M. L. Nordeen, D. Morstad, C. Nguyen, et al. (2013), Geostationary
859   enhanced temporal interpolation for CERES flux products, J. Atmos. Oceanic Technol., 30(6), 1072-1090,
860   https://doi.org/10.1175/JTECH-D-12-00136.1.
861   Donlon, C. J., P. J. Minnett, C. Gentemann, T. J. Nightingale, I. J. Barton, B. Ward, & M. J. Murray (2002), Toward
862   improved validation of satellite sea surface skin temperature measurements for climate research, J. Climate, 15(4),
863   353-369, https://doi.org/10.1175/1520-0442(2002)015<0353:tivoss>2.0.co;2
864   Dorman, C. E., A. G. Enriquez, & C. A. Friehe (1995), Structure of the lower atmosphere over the northern
865   California coast during winter, Mon. Wea. Rev., 123(8), 2384-2404, https://doi.org/10.1175/1520-
866   0493(1995)123<2384:SOTLAO>2.0.CO;2.
867   Douville, H., J. F. Royer, & J. F. Mahfouf (1995), A new snow parameterization for the Meteo-France climate
868   model, Climate Dynam, 12(1), 21-35, https://doi.org/10.1007/BF00208760.
869   Dubois, C., S. Somot, S. Calmanti, A. Carillo, M. Déqué, A. Dell'Aquilla, et al. (2012), Future projections of the
870   surface heat and water budgets of the Mediterranean Sea in an ensemble of coupled atmosphere–ocean regional
871   climate models, Climate Dynam, 39(7), 1859-1884, https://doi.org/10.1007/s00382-011-1261-4.
872   Ellingson, R. G. (1995), Surface longwave fluxes from satellite observations: A critical review, Remote Sens
873   Environ, 51(1), 89-97, https://doi.org/10.1016/0034-4257(94)00067-W.
874   Fasullo, J. T., J. Kiehl, K. E. Trenberth, & J. T. Fasullo (2009), Earth's Global Energy Budget, Bull. Amer. Meteor.
875   Soc., 90(3), 311-324, https://doi.org/10.1175/2008BAMS2634.1
876   info:doi/10.1175/2008BAMS2634.1.
877   Flerchinger, G. N., W. Xaio, D. Marks, T. J. Sauer, & Q. Yu (2009), Comparison of algorithms for incoming
878   atmospheric long-wave radiation, Water Resour Res, 45(3), https://doi.org/10.1029/2008wr007394.
879   Freitag, H. P. (1994), Calibration procedures and instrumental accuracy estimates of TAO temperature, relative
880   humidity and radiation measurements.
881   Freitag, H. P. (1999), COARE seacat data : Calibrations and quality control procedures,Producer.
882   Freitag, H. P. (2001), Calibration procedures and instrumental accuracies for ATLAS wind measurements,Producer.
883   Frouin, R., C. Gautier, & J. J. Morcrette (1988), Downward longwave irradiance at the ocean surface from satellite
884   data: Methodology and in situ validation, J Geophys Res-Oceans, 93(C1), 597-619,
885   https://doi.org/10.1029/JC093iC01p00597.
886   Fung, I. Y., D. E. Harrison, & A. A. Lacis (1984), On the variability of the net longwave radiation at the ocean
887   surface, Rev Geophys, 22(2), 177-193, https://doi.org/10.1029/RG022i002p00177.
888   Gelaro, R., W. McCarty, M. J. Suárez, R. Todling, A. Molod, L. Takacs, et al. (2017), The modern-era retrospective
889   analysis for research and applications, version 2 (MERRA-2), J. Climate, 30(14), 5419-5454,
890   https://doi.org/10.1175/Jcli-D-16-0758.1.

891 Grayek, S., J. Staneva, J. Schulz-Stellenfleth, W. Petersen, & E. V. Stanev (2011), Use of FerryBox surface
892 temperature and salinity measurements to improve model based state estimates for the German Bight, J Marine Syst,
893 88(1), 45-59, https://doi.org/10.1016/j.jmarsys.2011.02.020.
894 Gubler, S., S. Gruber, & R. S. Purves (2012), Uncertainties of parameterized surface downward clear-sky shortwave
895 and all-sky longwave radiation, Atmos. Chem. Phys., 12(11), 5077-5098, https://doi.org/10.5194/acp-12-5077-2012.
896 Guo, Y., J. Cheng, & S. Liang (2019), Comprehensive assessment of parameterization methods for estimating clear-
897 sky surface downward longwave radiation, Theoretical and Applied Climatology, 135(3), 1045-1058,
898 https://doi.org/10.1007/s00704-018-2423-7.
899 Habets, F., J. Noilhan, C. Golaz, J. P. Goutorbe, P. Lacarrère, E. Leblois, et al. (1999), The ISBA surface scheme in
900 a macroscale hydrological model applied to the Hapex-Mobilhy area: Part I: Model and database, Journal of
901 Hydrology, 217(1), 75-96, https://doi.org/10.1016/S0022-1694(99)00019-0.
902 Hack, J. J. (1998), Sensitivity of the simulated climate to a diagnostic formulation for cloud liquid water, J. Climate,
903 11(7), 1497-1515, https://doi.org/10.1175/1520-0442(1998)011<1497:SOTSCT>2.0.CO;2.
904 Henderson‐Sellers, B. (1984), A new formula for latent heat of vaporization of water as a function of temperature,
905 Quart J Roy Meteor Soc, 110(466), 1186-1190, https://doi.org/10.1002/QJ.49711046626.
906 Hersbach, H., B. Bell, P. Berrisford, S. Hirahara, A. Horányi, J. Muñoz‐Sabater, et al. (2020), The ERA5 global
907 reanalysis, Quart J Roy Meteor Soc, 146(730), 1999-2049, https://doi.org/10.1002/qj.3803.
908 Hoffmann, L., G. Günther, D. Li, O. Stein, X. Wu, S. Griessbach, et al. (2019), From ERA-Interim to ERA5: the
909 considerable impact of ECMWF's next-generation reanalysis on Lagrangian transport simulations, Atmos. Chem.
910 Phys., 19(5), 3097-3124, https://doi.org/10.5194/acp-19-3097-2019.
911 Idso, S. B., & R. D. Jackson (1969), Thermal radiation from the atmosphere, J. Geophys. Res., 74(23), 5397-5403,
912 https://doi.org/10.1029/JC074i023p05397.
913 Iziomon, M. G., H. Mayer, & A. Matzarakis (2003), Downward atmospheric longwave irradiance under clear and
914 cloudy skies: Measurement and parameterization, J Atmos Sol-Terr Phy, 65(10), 1107-1116,
915 https://doi.org/doi:10.1016/j.jastp.2003.07.007.
916 Jiang, B., S. Liang, H. Ma, X. Zhang, Z. Xiao, X. Zhao, et al. (2016), GLASS daytime all-wave net radiation
917 product: Algorithm development and preliminary validation, Remote Sens-Basel, 8(3),
918 https://doi.org/10.3390/rs8030222.
919 Jiang, B., Y. Zhang, S. Liang, G. Wohlfahrt, A. Arain, A. Cescatti, et al. (2015), Empirical estimation of daytime net
920 radiation from shortwave radiation and ancillary information, Agr Forest Meteor., 211-212, 23-36,
921 https://doi.org/10.1016/j.agrformet.2015.05.003.
922 Josey, S. A. (2003), A new formula for determining the atmospheric longwave flux at the ocean surface at mid-high
923 latitudes, J Geophys Res-Oceans, 108(C4), https://doi.org/10.1029/2002jc001418.
924 Josey, S. A., D. Oakley, & R. W. Pascal (1997), On estimating the atmospheric longwave flux at the ocean surface
925 from ship meteorological reports, J Geophys Res-Oceans, 102(C13), 27961-27972,
926 https://doi.org/10.1029/97jc02420.
927 Jost, G., R. Dan Moore, M. Weiler, D. R. Gluns, & Y. Alila (2009), Use of distributed snow measurements to test
928 and improve a snowmelt model for predicting the effect of forest clear-cutting, Journal of Hydrology, 376(1), 94-
929 106, https://doi.org/10.1016/j.jhydrol.2009.07.017.
930 Kjaersgaard, J. H., F. L. Plauborg, & S. Hansen (2007), Comparison of models for calculating daytime long-wave
931 irradiance using long term data set, Agr Forest Meteor., 143(1-2), 49-63,
932 https://doi.org/10.1016/j.agrformet.2006.11.007.
933 Lake, B. J. (2003), Calibration procedures and instrumental accuracy estimates of ATLAS air temperature and
934 relative humidity measurements, NOAA Tech. Memo. OAR PMEL-123, 23.
935 Li, M., & C. F. M. Coimbra (2019), On the effective spectral emissivity of clear skies and the radiative cooling
936 potential of selectively designed materials, Int J Heat Mass Tran, 135, 1053-1062,
937 https://doi.org/https://doi.org/10.1016/j.ijheatmasstransfer.2019.02.040.
938 Li, M., Y. Jiang, & C. F. M. Coimbra (2017), On the determination of atmospheric longwave irradiance under all-
939 sky conditions, Solar Energy, 144, 40-48, https://doi.org/https://doi.org/10.1016/j.solener.2017.01.006.
940 Lindau, R. (2012), *Climate atlas of the Atlantic Ocean: derived from the comprehensive ocean atmosphere data set*
941 *(COADS)*, Springer Science & Business Media.
942 Lohmann, D., E. Raschke, B. Nijssen, & D. P. Lettenmaier (1998), Regional scale hydrology: II. Application of the
943 VIC-2L model to the Weser River, Germany, Hydrological sciences journal, 43(1), 143-158,
944 https://doi.org/10.1080/02626669809492108.
945 McPhaden, M. J., K. Ando, B. Bourles, H. P. Freitag, R. Lumpkin, Y. Masumoto, et al. (2010), The global tropical
946 moored buoy array, Proceedings of OceanObs, 9, 668-682.

947 McPhaden, M. J., A. J. Busalacchi, R. Cheney, J. R. Donguy, K. S. Gage, D. Halpern, et al. (1998), The Tropical
948 Ocean-Global Atmosphere observing system: A decade of progress, J Geophys Res-Oceans, 103(C7), 14169-14240,
949 https://doi.org/10.1029/97JC02906.
950 McPhaden, M. J., G. Meyers, K. Ando, Y. Masumoto, V. S. N. Murty, M. Ravichandran, et al. (2009), RAMA: the
951 research moored array for African–Asian–Australian monsoon analysis and prediction, Bull. Amer. Meteor. Soc.,
952 90(4), 459-480, https://doi.org/10.1175/2008bams2608.1.
953 Medovaya, M., D. E. Waliser, R. A. Weller, & M. J. McPhaden (2002), Assessing ocean buoy shortwave
954 observations using clear-sky model calculations, J Geophys Res-Oceans, 107,
955 https://doi.org/10.1029/2000JC000558.
956 Meyers, T. P., & R. F. Dale (1983), PREDICTING DAILY INSOLATION WITH HOURLY CLOUD HEIGHT
957 AND COVERAGE, J Clim Appl Meteorol, 22(4), 537-545, https://doi.org/10.1175/1520-
958 0450(1983)022<0537:pdiwhc>2.0.co;2.
959 Mills, G. (1997), An urban canopy-layer climate model, Theoretical and applied climatology, 57(3), 229-244,
960 https://doi.org/10.1007/BF00863615.
961 Mousavi Maleki, S., H. Hizam, & C. Gomes (2017), Estimation of Hourly, Daily and Monthly Global Solar
962 Radiation on Inclined Surfaces: Models Re-Visited, Energies, 10(1), https://doi.org/10.3390/en10010134.
963 Moyer, K. A., & R. A. Weller (1997), Observations of surface forcing from the Subduction Experiment: A
964 comparison with global model products and climatological datasets, J. Climate, 10(11), 2725-2742,
965 https://doi.org/10.1175/1520-0442(1997)010<2725:OOSFFT>2.0.CO;2.
966 Nandan, R., M. V. Ratnam, V. R. Kiran, & D. N. Naik (2022), Retrieval of cloud liquid water path using radiosonde
967 measurements: Comparison with MODIS and ERA5, J Atmos Sol-Terr Phy, 227,
968 https://doi.org/10.1016/j.jastp.2021.105799.
969 Nice, K. A., A. M. Coutts, & N. J. Tapper (2018), Development of the VTUF-3D v1.0 urban micro-climate model to
970 support assessment of urban vegetation influences on human thermal comfort, Urban Climate, 24, 1052-1076,
971 https://doi.org/10.1016/j.uclim.2017.12.008.
972 Ogunjobi, K. O., & Y. J. Kim (2004), Ultraviolet (0.280–0.400 μm) and broadband solar hourly radiation at
973 Kwangju, South Korea: analysis of their correlation with aerosol optical depth and clearness index, Atmos Res,
974 71(3), 193-214, https://doi.org/10.1016/j.atmosres.2004.05.001.
975 Oleson, K. W., G. B. Bonan, J. Feddema, M. Vertenstein, & C. S. B. Grimmond (2008), An Urban Parameterization
976 for a Global Climate Model. Part I: Formulation and Evaluation for Two Cities, J. Appl. Meteor. Climatol., 47(4),
977 1038-1060, https://doi.org/10.1175/2007JAMC1597.1.
978 Pascal, R. W., & S. A. Josey (2000), Accurate Radiometric Measurement of the Atmospheric Longwave Flux at the
979 Sea Surface, J. Atmos. Oceanic Technol., 17(9), 1271-1282, https://doi.org/10.1175/1520-
980 0426(2000)017<1271:ARMOTA>2.0.CO;2.
981 Paul, B. (2021), Retrospective on the resource for radiative cooling, Journal of Photonics for Energy, 11(4), 042106,
982 https://doi.org/10.1117/1.JPE.11.042106.
983 Pauwels, V. R. N., N. E. C. Verhoest, G. J. M. De Lannoy, V. Guissard, C. Lucau, & P. Defourny (2007),
984 Optimization of a coupled hydrology–crop growth model through the assimilation of observed soil moisture and leaf
985 area index values using an ensemble Kalman filter, Water Resour Res, 43(4),
986 https://doi.org/10.1029/2006WR004942.
987 Payne, R. E. (1972), Albedo of the sea surface, J Atmos Sci, 29(5), 959-970, https://doi.org/10.1175/1520-
988 0469(1972)029<0959:AOTSS>2.0.CO;2
989 Payne, R. E., & S. P. Anderson (1999), A new look at calibration and use of Eppley precision infrared radiometers.
990 Part II: Calibration and use of the Woods Hole Oceanographic Institution improved meteorology precision infrared
991 radiometer, J. Atmos. Oceanic Technol., 16(6), 739-751, https://doi.org/10.1175/1520-
992 0426(1999)016<0739:ANLACA>2.0.CO;2.
993 Pinardi, N., I. Allen, E. Demirov, P. De Mey, G. Korres, A. Lascaratos, et al. (2003), The Mediterranean ocean
994 forecasting system: first phase of implementation (1998–2001), Annales Geophysicae, 21(1), 3-20,
995 https://doi.org/10.5194/angeo-21-3-2003.
996 Pinker, R. T., A. Bentamy, K. B. Katsaros, Y. Ma, & C. Li (2014), Estimates of net heat fluxes over the Atlantic
997 Ocean, J Geophys Res-Oceans, 119(1), 410-427, https://doi.org/10.1002/2013JC009386.
998 Pinker, R. T., B. Zhang, R. A. Weller, & W. Chen (2018), Evaluating Surface Radiation Fluxes Observed From
999 Satellites in the Southeastern Pacific Ocean, Geophys Res Lett, 45(5), 2404-2412,
1000 https://doi.org/10.1002/2017gl076805.
1001 Prata, A. (1996), A new longwave formula for estimating downward clear‐sky radiation at the surface, Quart J Roy
1002 Meteor Soc, 122(533), 1127-1151, https://doi.org/10.1002/qj.49712253306Citations: 348.

Rigon, R., G. Bertoldi, & T. M. Over (2006), GEOtop: A distributed hydrological model with coupled water and energy budgets, Journal of Hydrometeorology, 7(3), 371-388, https://doi.org/10.1175/JHM497.1.

Robinson, G. D. (1947), Notes on the measurement and estimation of atmospheric radiation, Quart J Roy Meteor Soc, 73(315‐316), 127-150, https://doi.org/10.1002/qj.49707331510.

Robinson, G. D. (1950), Notes on the measurement and estimation of atmospheric radiation–2, Quart J Roy Meteor Soc, 76(327), 37-51, https://doi.org/10.1002/qj.49707632705.

Rossow, W. B., & Y. C. Zhang (1995), Calculation of surface and top of atmosphere radiative fluxes from physical quantities based on ISCCP data sets: 2. Validation and first results, J Geophys Res-Atmos, 100(D1), 1167-1197, https://doi.org/10.1029/94JD02746.

Rutan, D. A., S. Kato, D. R. Doelling, F. G. Rose, L. T. Nguyen, T. E. Caldwell, & N. G. Loeb (2015), CERES synoptic product: Methodology and validation of surface radiant flux, J. Atmos. Oceanic Technol., 32(6), 1121-1143, https://doi.org/10.1175/JTECH-D-14-00165.1.

Saltelli, A., S. Tarantola, & K.-S. Chan (1999), A quantitative model-independent method for global sensitivity analysis of model output, Technometrics, 41(1), 39-56, https://doi.org/10.2307/1270993

Satterlund, D. R. (1979), IMPROVED EQUATION FOR ESTIMATING LONG-WAVE-RADIATION FROM THE ATMOSPHERE, Water Resour Res, 15(6), 1649-1650, https://doi.org/10.1029/WR015i006p01649.

Saucier, F. J., F. Roy, D. Gilbert, P. Pellerin, & H. Ritchie (2003), Modeling the formation and circulation processes of water masses and sea ice in the Gulf of St. Lawrence, Canada, J Geophys Res-Oceans, 108(C8), https://doi.org/10.1029/2000JC000686.

Schlosser, C. A., A. Robock, K. Y. Vinnikov, N. A. Speranskaya, & Y. Xue (1997), 18-Year Land-Surface Hydrology Model Simulations for a Midlatitude Grassland Catchment in Valdai, Russia, Mon. Wea. Rev., 125(12), 3279-3296, https://doi.org/10.1175/1520-0493(1997)125<3279:YLSHMS>2.0.CO;2.

Schulz, E. W., S. A. Josey, & R. Verein (2012), First air-sea flux mooring measurements in the Southern Ocean, Geophys Res Lett, 39(16), n/a-n/a, https://doi.org/10.1029/2012gl052290.

Schwarzschild, K. (1914), *Ueber Diffusion und Absorption in der Sonnenatmosphäre*.Sridhar, V., & R. L. Elliott (2002), On the development of a simple downwelling longwave radiation scheme, Agr Forest Meteor., 112(3), 237-243, https://doi.org/10.1016/S0168-1923(02)00129-6.

Staley, D. O., & G. M. Jurica (1972), Effective Atmospheric Emissivity under Clear Skies, J Appl Meteorol, 11(2), 349-356, https://doi.org/10.1175/1520-0450(1972)011<0349:EAEUCS>2.0.CO;2.

Swinbank, W. C. (1963), Long‐wave radiation from clear skies, Quart J Roy Meteor Soc, 89(381), 339-348, https://doi.org/10.1002/qj.49708938105.

Thandlam, V., & H. Rahaman (2019), Evaluation of surface shortwave and longwave downwelling radiations over the global tropical oceans, SN Applied Sciences, 1(10), https://doi.org/10.1007/s42452-019-1172-2.

Tiedtke, M. (1993), Representation of Clouds in Large-Scale Models, Mon. Wea. Rev., 121(11), 3040-3061, https://doi.org/10.1175/1520-0493(1993)121<3040:ROCILS>2.0.CO;2.

Vanhellemont, Q. (2020), Automated water surface temperature retrieval from Landsat 8/TIRS, Remote Sens Environ, 237, https://doi.org/10.1016/j.rse.2019.111518.

Vertessy, R. A., T. J. Hatton, P. J. O'Shaughnessy, & M. D. A. Jayasuriya (1993), Predicting water yield from a mountain ash forest catchment using a terrain analysis based catchment model, Journal of Hydrology, 150(2), 665-700, https://doi.org/10.1016/0022-1694(93)90131-R.

Viúdez-Mora, A., M. Costa-Surós, J. Calbó, & J. A. González (2015), Modeling atmospheric longwave radiation at the surface during overcast skies: The role of cloud base height, J Geophys Res-Atmos, 120(1), 199-214, https://doi.org/10.1002/2014jd022310.

Wang, K., & S. Liang (2009a), Global atmospheric downward longwave radiation over land surface under all-sky conditions from 1973 to 2008, J Geophys Res-Atmos, 114(D19), https://doi.org/https://doi.org/10.1029/2009JD011800.

Wang, T., J. Shi, Y. Ma, H. Letu, & X. Li (2020), All-sky longwave downward radiation from satellite measurements: General parameterizations based on LST, column water vapor and cloud top temperature, ISPRS Journal of Photogrammetry and Remote Sensing, 161, 52-60, https://doi.org/10.1016/j.isprsjprs.2020.01.011.

Wang, W., & S. Liang (2009b), Estimation of high-spatial resolution clear-sky longwave downward and net radiation over land surfaces from MODIS data, Remote Sens Environ, 113(4), 745-754, https://doi.org/10.1016/j.rse.2008.12.004.

Xu, J., Liang, S., Ma, H., He, T., Zhang, Y., & Zhang, G. (2023). A daily 5-km all-sky sea-surface longwave radiation product based on statistically modified deep neural network and spatiotemporal analysis for 1981–2018. *Remote Sensing of Environment*, *290*. https://doi.org/10.1016/j.rse.2023.113550

1059 Yang, F., & J. Cheng (2020), A framework for estimating cloudy sky surface downward longwave radiation from
1060 the derived active and passive cloud property parameters, Remote Sens Environ, 248,
1061 https://doi.org/10.1016/j.rse.2020.111972.
1062 Young, A. H., K. R. Knapp, A. Inamdar, W. Hankins, & W. B. Rossow (2018), The international satellite cloud
1063 climatology project H-Series climate data record product, Earth System Science Data, 10(1), 583-593,
1064 https://doi.org/10.5194/essd-10-583-2018.
1065 Yu, S., X. Xin, Q. Liu, H. Zhang, & L. Li (2018), Comparison of Cloudy-Sky Downward Longwave Radiation
1066 Algorithms Using Synthetic Data, Ground-Based Data, and Satellite Data, J Geophys Res-Atmos, 123(10), 5397-
1067 5415, https://doi.org/10.1029/2017jd028234.
1068 Zapadka, T., S. B. Woźniak, & B. Woźniak (2001), A simple formula for the net long-wave radiation flux in the
1069 Southern Baltic Sea, Oceanologia, 43(3), 265-277.
1070 Zeng, Q., Cheng, J., & Dong, L. (2020). Assessment of the Long-Term High-Spatial-Resolution Global LAnd
1071 Surface Satellite (GLASS) Surface Longwave Radiation Product Using Ground Measurements. *IEEE Journal of*
1072 *Selected Topics in Applied Earth Observations and Remote Sensing*, *13*, 2032–2055. IEEE Journal of Selected
1073 Topics in Applied Earth Observations and Remote Sensing. https://doi.org/10.1109/JSTARS.2020.2992472
1074 Zhou, Y., & R. D. Cess (2001), Algorithm development strategies for retrieving the downwelling longwave flux at
1075 the Earth's surface, J Geophys Res-Atmos, 106(D12), 12477-12488, https://doi.org/10.1029/2001jd900144.
1076 Zhou, Y., D. P. Kratz, A. C. Wilber, S. K. Gupta, & R. D. Cess (2007), An improved algorithm for retrieving
1077 surface downwelling longwave radiation from satellite measurements, J Geophys Res-Atmos, 112(D15),
1078 https://doi.org/10.1029/2006jd008159.
1079